Functionalization of thiosemicarbazide/gellan gum for the enhancement of cadmium removal from aqueous solutions – Grafting of tributyl phosphate derivative

Mohammed Hamza, Guibal Eric, Yuezhou Wei, Amr Fouda, Khalid Althumayri, Hanaa Abu Khoziem, Noha Mashaal

Functionalization of thiosemicarbazide/gellan gum for the enhancement of cadmium removal from aqueous solutions – Grafting of tributyl phosphate derivative

Mohammed F. Hamza [a,b], Eric Guibal [c,*], Yuezhou Wei [a,d,*], Amr Fouda [e], Khalid Althumayri [f], Hanaa A. Abu Khoziem [b], Noha M. Mashaal [g]

[a] School of Nuclear Science and Technology, University of South China, Heng Yang 421001, China
[b] Nuclear Materials Authority, POB 530, El-Maadi, Cairo, Egypt
[c] Polymers Composites and Hybrids (PCH), IMT Mines Ales, Alès, France
[d] School of Nuclear Science and Engineering, Shanghai Jiao Tong University, Shanghai, China
[e] Botany and Microbiology Department, Faculty of Science, Al-Azhar University, Nasr City, Cairo 11884, Egypt
[f] Department of Chemistry, College of Science, Taibah University, 30002 Al-Madinah Al-Munawarah, Saudi Arabia
[g] Department of Geology, Faculty of Science, Menoufia University, Shibin El-Kom, Egypt

A B S T R A C T

Two sorbents are successfully synthesized based on the chemical modification of gellan gum (GG). First, thio-semicarbazide is grafted onto GG to produce GEG-C. In a second step, GEG-C is functionalized with a derivative of tributyl phosphate (dTBP, giving GEG-P sorbent). The sorption properties are compared for recovery of Cd(II) from aqueous solutions. GEG-C is expected to bind Cd(II) through carboxylic, amine, and thiocarbonyl groups, while phosphate groups in GEG-P contribute to increase metal sorption. The chemical modification improves not only the uptake kinetics (equilibrium time ≈30 min, vs. 45 min) but also the sorption capacities (≈2.79 vs. 1.60 mmol Cd g^{-1}), at optimum pH (i.e., pH 5). The functionalization also improves (a) the sorbent stability (weaker reduction of the loss in sorption efficiency after five cycles of reuse compared with GEG-C) and (b) the sorption selectivity in the presence of competitor ions (from equimolar multicomponent solutions), especially at pH 4. Different sorption mechanisms may be involved depending on the pH (deprotonation of reactive groups) including chelation (onto deprotonated amine and phosphonate groups) and ion exchange (protonated groups with metal cations). Cadmium sorption is reversed by contact with 0.3 M HCl solution. The functionalization (GEG-P) strongly increases the selectivity coefficient for Cd(II) against major elements in mining effluent, especially at pH higher than 5. These results confirm the interest of multifunctionality in the development of new sorbents based on renewable resources (such as gellan gum).

Keywords:
Cadmium(II) sorption
Uptake kinetics
Sorbent recycling
Sulfur derivative of gellan gum
TBP-functionalization
Selective separation

1. Introduction

The anthropogenic activities, as well as the effects of erosion or weathering, may cause strong contamination of water bodies by metal contamination with direct impact on plants and agriculture, water drinking quality, and *in fine* on the health of living beings (animals and humans). Cadmium is part of these hazardous contaminants. For example, due to its long half-life in human body (about 10–35 years) [1], it may have strong impact on health. Hence, cadmium is recognized as a potential carcinogenic vector (especially by inhalation); however, the kidney is the main target organ for cadmium toxicity [2–4]. The World Health Organization set the guideline value for cadmium to 3 μg L^{-1} in drinking water [1]. Up to recently, 80 % of used cadmium concerned the sector of batteries (nickel-cadmium batteries, [5]); this part tends to decrease to face the hazardous impacts of battery discharge to the environment, being replaced with nickel metal hydride batteries. For similar reasons, the use of cadmium in pigments and cathodic tubes strongly decreased. However, some sectors such as electroplate steel, and corrosion-protected metal pieces (alloying uses), solar cells, plastic stabilizers, and nuclear industry (as atomic fission controller) still use cadmium [6]. This makes cadmium a widely used hazardous metal.

The removal of cadmium is thus of critical importance for

* Corresponding authors.
E-mail addresses: eric.guibal@mines-ales.fr (E. Guibal), yzwei@usc.edu.cn (Y. Wei).

minimizing environmental and health impacts both in terms of industrial discharges (end of pipe) and drinking water supply. The target of the current study focuses on the treatment of industrial waste flows (processed water, leachates in the treatment of WEEE (waste from electrical and electronic equipment) and batteries, metal removal from mining effluents, etc.) rather than drinking water application.

For the treatment of non-trace Cd-bearing effluents, several techniques can be scanned [7], including specific precipitation sequence [8], phosphate-based precipitation [9], or sulfide precipitation [10]. Solvent extraction is also frequently used for purifying phosphoric acid solutions or removing cadmium from concentrated complex effluents [7,11–13]. However, for less-concentrated effluents, the use of sorption processes is usually preferred. A wide range of sorbents more or less sophisticated has been investigated for the last decade: nano-scale materials such metal oxides [14], metal-oxide supported carbon nanofibers [15], carbon-based sorbents [16,17], but also agriculture wastes [18], or derivatives of these agriculture resources [19], microbial biomass [20], seaweed sub-products [21], or polysaccharides [22]. Conventional ion-exchange and chelating resins have also received a great attention playing with the diversity of functional groups such as sulfonic acid groups [23–26], dual sulfonic/phosphonic groups [27], and amine/thiol groups [28]. The selectivity performance may be enhanced by cadmium ion-imprinting procedure [29]; while the immobilization of extractant in porous supports combines the efficiency of solvent extraction systems and the retention capability and easy application modes of resins for improved extraction performance [30–32]. Tributyl phosphate has shown great affinity for cadmium recovery in solvent extraction processes [33–35].

There is a strong research for substituting petro-sourced supports with naturally occurring polymers for developing alternate sorbents. Chitosan, alginate, and cellulose have retained a great attention because of the presence of readily modifiable functional moieties such as amine, carboxylic, or hydroxyl groups, in addition to their proper reactivity for metal ions (through different mechanisms such as chelation or ion exchange) [36–40]. However, alternative biopolymers recently gained increasing interest such as gums [41]. Among these natural gums extracted from plants, microorganisms, and trees, gellan gum reveals very promising based on its ability to form stable blends with different types of polymers [42,43]. Gellan gum is an anionic polysaccharide constituted of D-glucose units, associated with L-rhamnose and D-glucuronic acid units ($[$D-Glc($\beta1 \rightarrow 4$)D-GlcA($\beta1 \rightarrow 4$)D-Glc($\beta1 \rightarrow 4$)L-Rha($\alpha1 \rightarrow 3$)$]_n$). The presence of carboxylic groups naturally offers the possibility to bind metal ions: for example, the sorption capacity of gellan gum beads reach up to 0.62 mmol Cd g^{-1} [44]. The biopolymer has been used for designing different composite sorbents associating for example synthetic polymers [45–48], graphene oxide [49,50]. Hereafter, gellan gum (GEG) is chemically modified by reaction of thiosemicarbazide through the crosslinking action of epichlorohydrin (EPI, by ring opening polymerization) [51]. This functionalization (GEG-C) both improves the stability of the support (cross-linking) and the immobilization of new reactive groups (amine and thiocarbonyl groups) for enhancing the binding of metal ions (through different modes of interaction). In a second step, the GEG-C sorbent is functionalized with phosphate moieties through the grafting of a derivative of tributyl phosphate (TBP), which is obtained by reaction with phosphoric acid (to form dibutylphosphate), followed by the reaction with epichlorohydrin; this reaction forms an activated phosphate compound (dibutyl-(3-chloro-2_hydroxy)-propyl phosphate, DBCHPP). The final sorbent (GEG-P) is a multi-functional sorbent bearing a high density of phosphate groups and completed with thiocarbonyl and amine groups. The multi-functionality has shown interesting properties for enhancing the sorption performances of resins by modulation of hydrophilic/hydrophobic, acid-base, conformational properties [52] or synergistic effects [53].

The objective of the current work focuses on the comparison of sorption properties of GEG-C and GEG-P sorbents for the removal of cadmium from aqueous solutions. Is the chemical modification (of increasing complexity) improving significantly the sorption performances of the material in terms of sorption capacity (isotherms), kinetics of uptake, pH range of activity, stability, and selectivity? After characterizing the materials and their interactions with cadmium, the sorption properties are first investigated in synthetic solutions (mono-component and multi-metal solutions) before applying the sorption process to industrial effluents.

2. Materials and methods

2.1. Materials

Gellan gum (GEG) was purchased from Gino Biotech (Zhengzhou, Henan, China). Epichlorohydrin (EPI, 99 %), tributyl phosphate (TBP, >99 %), ethanol (EtOH, 95 %) and phosphoric acid (99.99 %) were supplied by Shanghai Makclin Biochemical Co., Ltd. (Shanghai, China). Thiosemicarbazide (TSCZ, 99 %), acetone (>99.5 %), sodium hydroxide (≥97.0 %), and hydrochloric acid (37 %) were purchased from Sigma-Aldrich (Merck KGa, Darmstadt, Germany). Cadmium(II) chloride hydrated (99.0 %), sodium chloride (≥99.0 %)*, calcium(II) chloride (≥99.1 %)*, magnesium(II) chloride (95.0 %)*, iron(III) chloride (≥98.0 %)*, aluminum(III) chloride (≥99.0 %)*, zinc(II) chloride (≥98.0 %)*, and lead(II) chloride (98.0 %)* were supplied by Sigma Aldrich (Shanghai-Trading Co., Ltd., Pudong, Shanghai China). Other chemicals and reagents used in the study were acquired from Prolabo products (VWR, Radnor, PA, USA). * Reagents specifically used for selectivity tests.

2.2. Synthesis of sorbents

2.2.1. Synthesis of the phosphorylating agent (dibutyl-(3-chloro-2-hydroxy)-propyl phosphate, DBCHPP)

The synthesis of the phosphorylating agent was optimized and described in a previous work [54]. Briefly, TBP (34 g) was mixed with H_3PO_4 (12.6 g) under reflux (at 80–85 °C) for 1 h. After cooling, EPI (12 g) was progressively (for 30 min) added to the mixture under stirring. The system was maintained for further 4 h at 85–90 °C; the oily liquid was washed with acetone and benzene for removing the impurities and producing the phosphorylating agent (23 mL) [55].

2.2.2. Synthesis of the pristine composite: GEG-C (non-functionalized composite)

Gellan Gum (GEG, 4 g) was mixed with 1.0 g of thiosemicarbazide (TSCZ) in 50 mL of ethanol; the pH was adjusted to 9 using 5 M NaOH solution, before progressively dropping 5 mL of EPI (excess amount, for 5 min). The mixture was maintained under stirring (and condenser) at 40 °C for 12 h. The precipitate (appearing as a hydrogel) was collected by filtration and washed with acetone, before being dried. The yield of GEG-C synthesis reached 8.9 g (meaning conversion ≈89 %, based on weight increase).

2.2.3. Synthesis of functionalized sorbent: GEG-P

For the phosphorylation of GEG-C, the polymer (5 g) was soaked in 50 mL of toluene before adding the phosphorylating agent (23 mL). The mixture was stirred under reflux for 12 h (T: 70–75 °C). The phosphorylated composite (GEG-P) was filtrated and washed with acetone, and finally dried at 60 °C for 12 h. The yield was 9.3 g.

Scheme 1 summarizes the different steps in the synthesis of GEG-C and GEG-P sorbents.

2.3. Characterization of materials

Nitrogen adsorption-desorption isotherms were acquired at 77 K (after degassing for 4 h at 110 °C) using a TriStar II surface area and porosity analyzer (Micromeritics, Norcross, GA, USA). The specific surface area (S_{BET}, $m^2\ g^{-1}$) was determined by the BET method, while

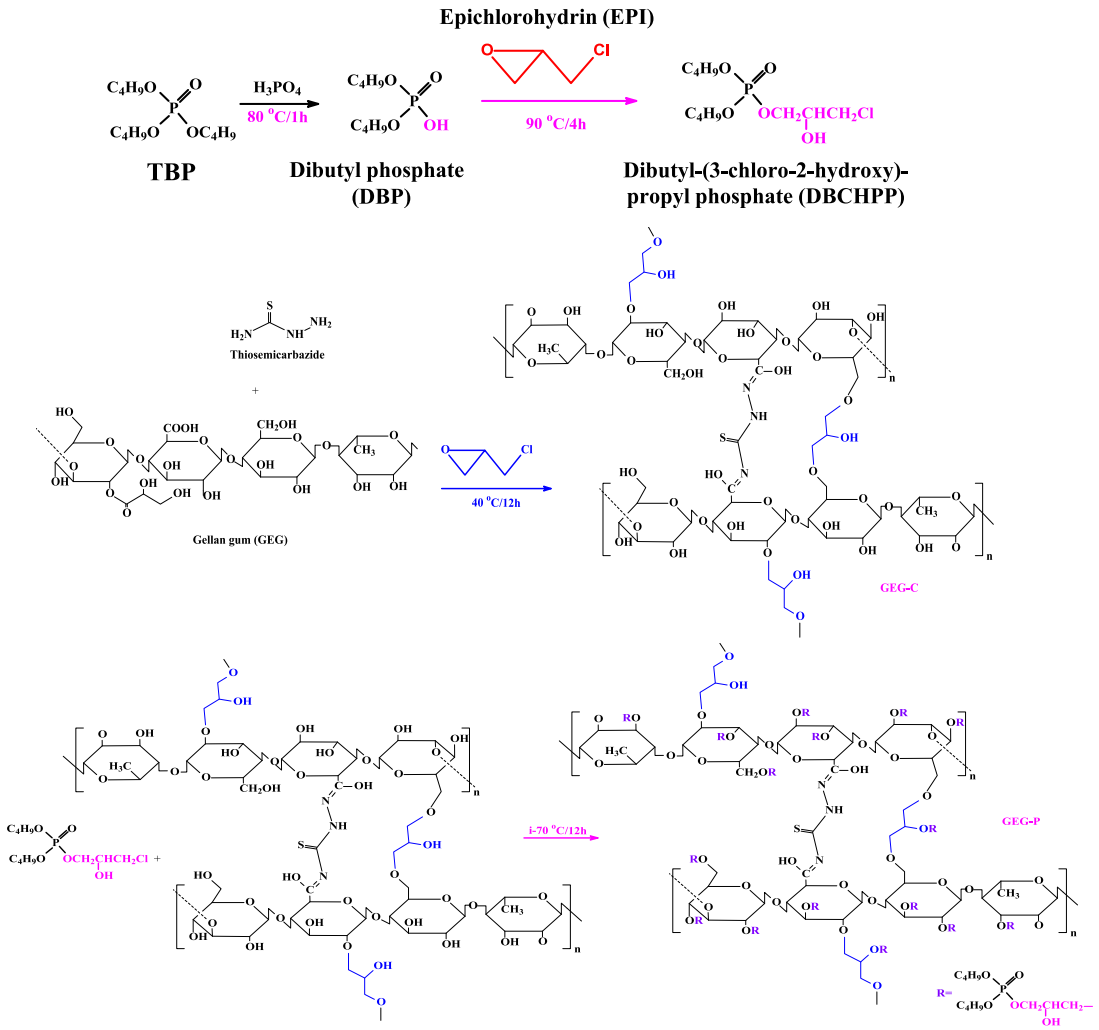

Scheme 1. Synthesis routes for DBCHPP (organophosphate substituent), GEG-C, and GEG-P sorbents.

the pore volume ($cm^3\ g^{-1}$) and the pore distribution (Å) were obtained by the BJH method. The morphology and the chemical composition of the materials were recorded using a Phenom ProX-SEM (scanning electron microscope, Thermo Fisher Scientific, Eindhoven, Netherlands) equipped with energy dispersive X-ray (EDX) spectroscopy tool. FTIR spectra of the samples (conditioned in KBr disc) were collected on IR-Tracer100 spectrometer (Shimadzu, Tokyo, Japan). The samples were analyzed by thermogravimetry under N_2 atmosphere with STA-449-F3 Jupiter thermal analyzer (Netzsch Gerätebau HGmbh, Selb, Germany); the temperature ramp was set at 10 °C min^{-1}. The elemental analysis of sorbent was processed using a Vario-EL cube (Elementar Analysensysteme GmbH, Langenselbold; Germany).

The pH-drift method was used for the determination of the pH of zero charge (pH_{pzc}) [56]. A fixed amount of sorbent was mixed with a series of solutions (with 0.1 M NaCl as the background salt) with initial pH (i.e., pH_0) varying between 1 and 11. The pH_{eq} of the solution, after 48 h of contact, was measured using a S220-Seven pH-ionometer (Mettler-Toledo, Shanghai, China). The pH_{PZC} value corresponds to the condition: $pH_0 = pH_{eq}$.

2.4. Sorption tests

2.4.1. Experimental procedures

The sorption (and desorption) studies were performed in batch systems. A fixed volume of solution (V, L) was mixed with a given amount of sorbent, m, g; i.e., sorbent dose, $SD = m/V$, g L^{-1}. For uptake kinetics and sorption isotherms (see below), the SD value was 0.667 g L^{-1} and 0.66 g L^{-1}, respectively. The solutions containing a fixed initial concentration of cadmium (C_0, mmol L^{-1}, and eventually other metal ions) were controlled at fixed pH values (pH_0) using 0.1–1 M NaOH or HCl solutions. The pH was not adjusted during sorption tests but the final pH (pH_{eq}) was systematically recorded. At fixed times (for uptake kinetics) or after 48 h of contact (for equilibrium tests and sorption isotherms) a sample was collected, filtrated (through 1.2-µm pore size filter membrane), and analyzed for residual concentration (C_{eq}, mmol L^{-1}) using an inductively coupled plasma atomic emission spectrometer (ICP-AES, ICPS-7510, Shimadzu Corporation, Kyoto, Japan). By the mass balance equation, the sorption capacity (q, mmol g^{-1}) was calculated according to: $q = (C_0\text{-}C_{eq}) \times V/m$. Similar experimental procedures were adopted for testing the sorption in multi-component solutions. For desorption tests, the samples collected at the end of uptake kinetics (with known metal content) were mixed with the eluent (herein 0.3 M HCl solution) with a SD of 2.64 g L^{-1}, for 2 h. The mass balance was used again for calculating the desorption yield. A rinsing step was systematically operated between each sorption and desorption steps in the study of sorbent recycling. The SD values for the sorption and desorption steps were 0.66 g L^{-1} and 2 g L^{-1}, respectively. The experimental conditions are systematically reported in the caption of the figures. Sorption tests were duplicated: the figures show the average values (with standard deviation).

The distribution ratio, D (L g^{-1}), is calculated as $D = q_{eq}/C_{eq}$. The selectivity coefficient for Cd over competitor metal (i.e., $SC_{Cd/metal}$) is

obtained from:

$$SC_{Cd/metal} = \frac{D_{Cd}}{D_{metal}} = \frac{q_{eq,Cd} \times C_{eq,metal}}{C_{eq,Cd} \times q_{eq,metal}} \quad (1)$$

Tables S1 and S2 report the equations used for fitting kinetic profiles and sorption isotherms, respectively. The profiles of uptake kinetics were analyzed using the pseudo-first (PFORE) and the pseudo-second (PSORE) order rate equations [57], and by the Crank equation (as a simplified equation simulating the resistance to intraparticle diffusion) [58]. For the fitting of sorption isotherms different models were tested: Langmuir, Freundlich, Sips [59], Temkin [60,61], Dubinin-Radushkevich (D-R) [62], and (when relevant) the Langmuir Dual Site (LDS) equations [63]. The non-linear regression analysis was used for evaluating the parameters of these equations (using Mathematica® facilities and proprietary notebook). The quality of the fits was compared between the different models using the determination coefficient (i.e., R^2) and the Akaike information criterion (AIC); the AIC values of two models are usually considered significantly different when $|\Delta(AIC)| \geq 2$.

2.5. Application to real effluent

The sorption properties of the two sorbents where tested on real mining effluents. The sample was used after membrane filtration (1.2-μm pore size). The actual pH of the solution was 5.83. Sorption tests were performed at different pH values (controlled with 0.1/1 M HCl solutions) under fixed experimental conditions (SD: 1.5 g L^{-1}; v: 210 rpm; contact time: 24 h; T: 21 ± 1 °C). After filtration (and measurement of the equilibrium pH), the residual concentrations were analyzed by ICP-AES for evaluation of sorption capacities for a series of metal ions (including cadmium, lead, zinc, copper, aluminum, and iron).

3. Results and discussion

3.1. Characterization of sorbents

3.1.1. SEM- and SEM-EDX analyses

The SEM observation of sorbent particles shows that the particles (which were grinded) are irregular with rounded edges, appearing as agglomerates of particles and plate-shaped objects (Fig. S1). In the case of GEG-C, the distribution of particle sizes shows two populations: large particles (7–12 μm) and small objects (1–8 μm). After functionalization (in GEG-P), smaller particles are observed (large majority of particles in the range 1–8 μm), though some aggregates can be observed (12–25 μm). The average values for GEG-C and GEG-P are close to 10 μm and 7 μm, respectively.

3.1.2. Textural properties

The adsorption and desorption isotherms of N_2 for GEG-C and GEG-P sorbents are remarkably close (superposed) (Fig. S2). This is confirmed by the evaluation of specific surface area; indeed, S_{BET} values reach 56.8 $m^2\ g^{-1}$ and 58.5 $m^2\ g^{-1}$, respectively (Fig. S2a). These profiles are characterized by a long p/p_0 linear range with a slow slope (up to $p/p_0 \approx 0.8$) at low sorbed volume (i.e., 10–60 $cm^3\ g^{-1}$) followed by a steep increase in the sorbed volume, with a hysteresis loop. This behavior can be associated with the Type IV(a) isotherm [64]. This kind of profile is usually associated with mesoporous materials having pore width relatively large (wider than 4 nm), and to capillary condensation mechanism. In addition, the hysteresis loop resembles the H1 loop described by Thommes et al. [64]; meaning that pore size distribution is narrow. It is noteworthy that high p/p_0 volume (above 0.97) the isotherms show unexpected trend with a new sharp increase and a gap between adsorption and desorption branches. The pore volume are also very close: 0.94 $cm^3\ g^{-1}$ for GEG-C and 1.03 $cm^3\ g^{-1}$ for GEG-P sorbents. The BJH analysis of pore size distribution gives pore width as large as 667–449 Å (values associated with the adsorption and desorption branches, respectively) for GEG-C and even higher as 725–486 Å for GEG-P. Fig. S2b shows the distributions of pore sizes with a narrow peak centered around 640–680 Å. This is consistent with the interpretation reported above (i.e., narrow pore size distribution), though Thommes et al. [64] reported much thinner pore size for systems characterized by H1-type hysteresis loops.

In the case of arginine-modified bentonite incorporated in gellan gum, Abbasi and Ikram [65] reported lower textural properties in terms of S_{BET} values (i.e., ≈14 $m^2\ g^{-1}$), pore volume (i.e., ≈0.04 $cm^3\ g^{-1}$), and pore size (i.e., ≈139 Å). In the case of gellan gum microspheres reinforced by carboxymethyl konjac glucomannan, the S_{BET} reached 21.5 $m^2\ g^{-1}$ (with pore size close to 44.5 Å) [66].

3.1.3. Thermogravimetric analysis

Fig. S3 compares the profiles for the thermal degradation of the two polymers (under N_2 atmosphere). This comparison may help in the confirmation of chemical modification of pristine sorbent but also in evaluating the strategies for thermal elimination of the sorbent at the end of its life cycle. In the case of GEG-C sorbent, two main steps are identified in terms of weight loss (Fig. S3a): (a) below 192 °C, GEG-C loses ≈16 % (essentially as release of adsorbed water), (b) above 192 °C (up to ≈620 °C), the sorbent loses about 77.6 %. The weight loss in this second step is almost homogeneous with two weak shoulders that are evidenced by the DTG curve (Fig. S3c) and two main endothermic peaks at 335.8 °C and 594.2 °C (a weaker shoulder appears at 478.4 °C). This may correspond to the depolymerization of the polymer, the degradation of thiosemicarbazide, the char formation (before its degradation). The final weight loss reaches up to 93.6 %. On the opposite hand, for GEG-P the total weight loss does not exceed 81 % (Fig. S3a). It is well known that the introduction of phosphorous-based compounds in polymers contributes to reinforce their thermal stability [67]. The profile of weight loss shows more marked thermal transitions: indeed, four steps can be identified: three major endothermic peaks can be identified at 321.4 °C, 510.4 °C, and 729.6 °C (less marked) (Fig. S3b). The change in the weight loss profile confirms the chemical modification of the pristine support (GEG-C). The phosphate groups increases the thermal stability of the functionalized sorbent as shown by both the increase in the residual mass at 800 °C and the shift of the last degradation step toward higher temperatures. Pandey et al. [45] compared the thermal degradation of gellan gum with that of gellan gum/*N*,*N*-dimethylacrylamide copolymer. After the loss of solvent (water, alcohol), the gellan gum degraded in a single step (at 237 °C) that begins at 102 °C, with a maximum rate of degradation at 256.6 °C (sharp endothermic peak). On the opposite hand, the grafted copolymer shows two steps of degradation with two maximum rates at 87.6 °C and 227.6 °C. These critical temperatures are substantially lower than those found for both GEG-C and GEG-P sorbents; meaning that the functionalization steps progressively increase sorbent stability. At the end of their life cycle, higher temperature will be necessary for achieving the thermal degradation of the sorbents.

3.1.4. FTIR spectroscopy

Fig. 1 summarizes the FTIR spectra of the two sorbents under different experimental conditions: the sorbents as-prepared, the sorbents after being conditioned at the pH of metal sorption, the sorbents after Cd(II) sorption, and after recycling (5th cycle). The sorption being operated at pH 5 (meaning not drastic conditions), the FTIR spectrum of GEG-C is poorly modified and the differences potentially observed between raw sorbent and after Cd(II) will be directly assigned to their proper reactivity with the metal ions. Differences are more marked in the case of GEG-P.

In the region 4000–2000 cm^{-1} (Fig. 1a,b), the spectra of GEG-C and GEG-P are substantially different. In GEG-C, a series of small bands in the range 3200–2800 cm^{-1} can be observed corresponding to $\nu_{C\text{-}H}$ vibrations (methoxy and methylene groups, at 2856, 2931, and 2985 cm^{-1}) and $\nu_{O\text{-}H}$ vibrations (at 3036 and 3095 cm^{-1}), completed by small "indents" at higher wavenumbers (probably associated with $\nu_{N\text{-}H}$

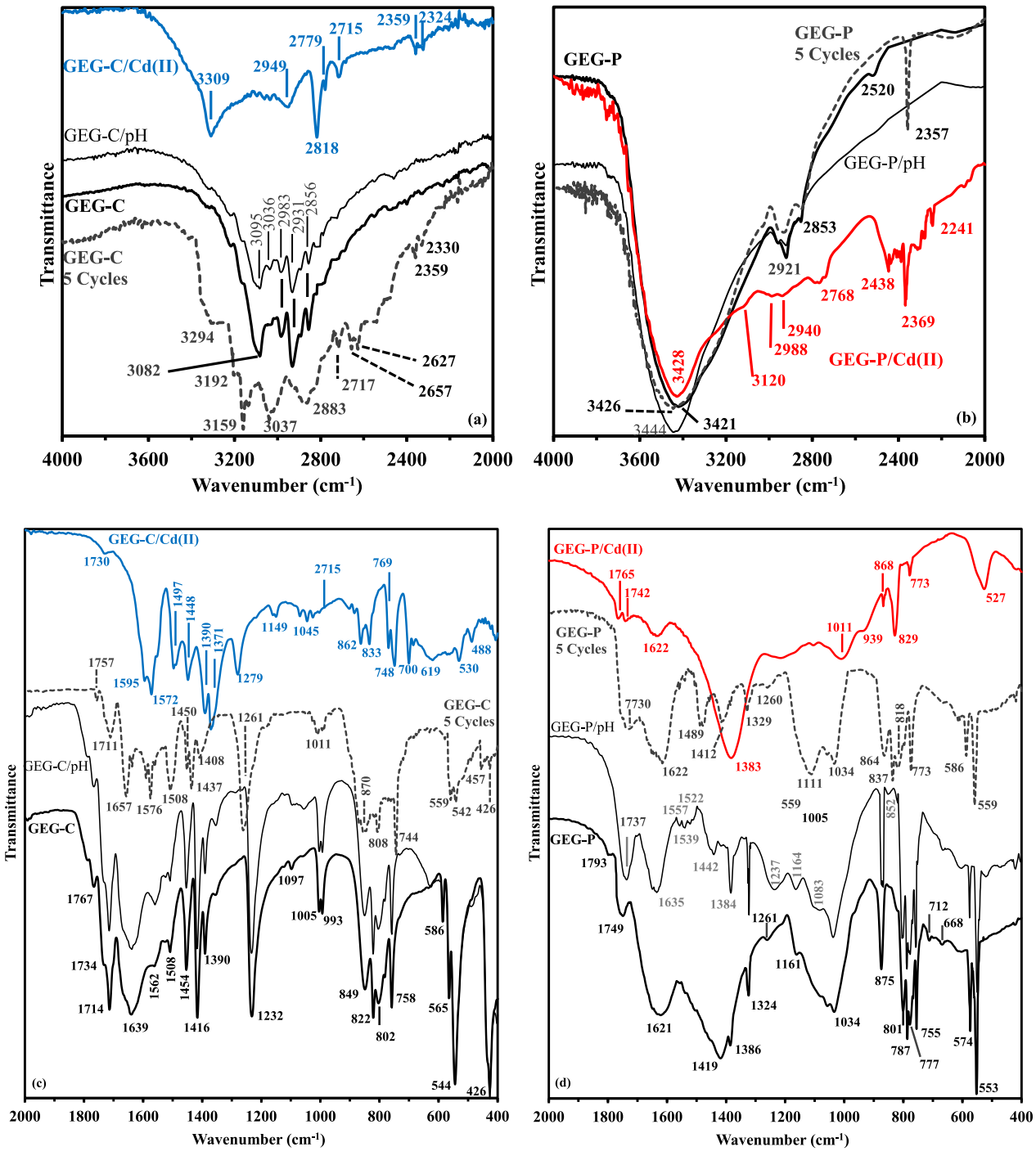

Fig. 1. FTIR spectra of GEG-C (a,c) and GEG-P (b,d) sorbents at different stages of use (pristine sorbents, after conditioning at the pH of sorption (sorbent/pH), after Cd(II) sorption, and after 5 cycles of sorption/desorption).

vibrations). In the case of GEG-P, the $\nu_{C\text{-}H}$ vibrations are clearly identified at 2853 and 2921 cm^{-1}; however, the bands in the region above 3000 cm^{-1} are replaced with a broad and poorly resolved band (centered around 3421 cm^{-1}) resulting from superposition of contributions from $\nu_{O\text{-}H}$ and $\nu_{N\text{-}H}$ vibrations. The band observed at 2520 cm^{-1} may be assigned to the tautomerization form of sulfone/amine moiety. Several reasons may explain the differences in the profiles: (a) the increase in the density of hydrocarbon groups (OBut), (b) the tautomerization of P═O converted to P-OH, (c) the presence of –OH (brought by the grafted moiety), and/or (d) the hydrogen bond between P═O and the adjacent –OH group.

The region 2000–400 cm^{-1} brings confirmation of the presence of typical reactive groups (Fig. 1c,d). The glycosidic bond is detected at 1639 and 1621 cm^{-1} (broader band) in GEG-C and GEG-P, respectively [68]. For the two sorbents, the band is broad and rounded by shoulders or small peaks; this may be explained by the superposition of the contribution of amine vibrations, including $\delta_{N\text{-}H}$ and $\nu_{C=N}$ vibrations [69], or imine vibration from thiosemicarbazide [70]. The $\nu_{C\text{-}C}$ vibrations here are observed at 1416 and 1419 cm^{-1}, respectively. This band is broad in the case of GEG-P probably due to the superposition of signals associated with the high density of propyl chains (in the grafted organophosphate compound) and more generally TBP characteristic

band at 1464 cm^{-1} [71]. The bands at 1767, 1734, and 1714 cm^{-1} are associated with carboxyl groups in GEG [72]. A series of bands are observed around 1000 cm^{-1} in GEG-C and in the range 850–700 cm^{-1}, which may be assigned to $\nu_{C\text{-}O\text{-}C}$ vibrations [72]. Around 1000 cm^{-1}, a very broad band is observed in the case of GEG-P; this can be assigned to the superposition of the $\nu_{P\text{-}O\text{-}C}$ vibration [69,71]. For both GEG-C and GEG-P, the strong bands observed at 544/553 cm^{-1} and 565/574 cm^{-1} may be attributed to $\nu_{N\text{-}C=S}$ vibrations [70]. The small band at 997 cm^{-1} in GEG-C ($\nu_{C=S}$ vibration) is masked in the spectrum of GEG-P. A new strong band appears at 875 cm^{-1}, which can be assigned to C-O band (which is shifted due to the presence of new groups from the phosphorylating agent; i.e., C-O(-P) and C-O(-H)).

After Cd(II) sorption, strong changes are observed in the FTIR spectra for both GEG-C and GEG-P sorbents. Hence, for GEG-C, the major changes concern the environment of carboxyl groups in the region 1800–1700 cm^{-1}: the bands disappear. The large band at 1639 cm^{-1} (glycosidic ring and amine groups) are shifted toward lower wavenumbers (with thinner bands at 1572 cm^{-1}, including a side band at 1595 cm^{-1}). There are several significant changes in the region 1500–1350 cm^{-1} that are also shifted to lower wavenumbers. The strong doublet at 565–544 cm^{-1} (associated with thiocarbonyl group in thiosemicarbazide linking) is drastically reduced after metal binding. These different changes suggest that Cd(II) sorption affects the chemical environment of the different reactive groups present on the sorbent, including carboxylate groups (from GEG), amine and sulfur groups (from thiosemicarbazide). In the case of GEG-P, it is noteworthy that the conditioning of the sorbent at the pH of sorption changes the environment of N-bearing groups (at 1621 cm^{-1}) and also the broad and poorly resolved band at 1419 cm^{-1} (where the superposed bands at 1570–1400 cm^{-1} are strongly reduced). The deprotonation of these reactive groups affects more significantly the spectrum of GEG-P than in the case of GEG-C (consistently with the difference in pH_{PZC} values, see below). However, despite these significant variations due to sorbent conditioning at pH 5, the sorption of cadmium involves additional significant changes in the FTIR spectrum with considerable decrease in intensity of the bands associated with carboxyl and amine groups in the region 1800–1300 cm^{-1}: small residues appear at 1765, 1742 (shifted from 1793 and 1749 cm^{-1}) and 1622 cm^{-1}. The band at 1419 cm^{-1} (with bands at 1386 and 1324 cm^{-1}, better resolved with two clear bands at 1442 and 1384 cm^{-1} after being pH-conditioned) is replaced with a strong symmetric and broad band at 1383 cm^{-1}; these changes are associated with the interaction of phosphate moieties with metal ion. The broad band at 1034 cm^{-1} (also assigned to phosphate moieties) is also strongly reduced (with a band centered around to 1011 cm^{-1}); the intensities of the series of bands at 875, 801, 787, 777, and 755 cm^{-1} are also considerably decreased with bands limited to 2 small peaks at 868 and 773 cm^{-1}, and largest contribution at 829 cm^{-1}. The 574–553 cm^{-1} doublet is replaced with a broad (and less intense) band shifted to 527 cm^{-1}. Consistently with GEG-C sorbent, the functionalized sorbent mobilizes carboxylate and N-bearing groups for Cd(II) binding, however, the phosphate reactive groups are also strongly engaged in metal sequestration.

The desorption of cadmium and the recycling of the sorbent (for five successive cycles) may affect the stability of the sorbent (degradation and/or protonation of reactive groups). Fig. 1c,d allows comparing the spectra of the recycled sorbent with the pristine sorbents. In the case of GEG-C, the spectrum is roughly restored; although some changes can be identified; especially in the region around 1639 cm^{-1} (due to the probable protonation of N-based sites), and the shift of the strong peak at 1232 cm^{-1} to 1261 cm^{-1}, as well as the quasi-disappearance of the bands at 586 and 426 cm^{-1}. This may be due to the protonation of groups associated with strong acidic condition in the desorption process. For GEG-P, the most significant changes are identified for: (a) the broad band at 1419 cm^{-1} (phosphate signal), which is replaced with resolved bands at 1489 and 1412 cm^{-1}, and (b) the broad band at 1161–1034 cm^{-1} (including $\nu_{P\text{-}O\text{-}C}$ vibration), which are replaced with two bands at 1111 and 1034 cm^{-1} (at lower relative intensity for the second band). In the case of functionalized sorbent, the recycling of the sorbent clearly shows that the environment of phosphate groups are affected. Apparently, these modifications hardly affect Cd(II) sorption performance (see below, Section 3.2.5.).

3.1.5. Elemental analysis and titration

The elemental analysis of GEG-C and GEG-P sorbents is summarized in Table S3. The presence of S element (0.97 % w/w, or 0.3 mmol S g^{-1}) confirms the reaction of thiosemicarbazide with gellan gum. The global observation of the composition shows that the contents of N and H are hardly varied by the functionalization of GEG-C. On the opposite hand, the grafting of DBCHPP is followed by a significant decrease in the relative contents of C (from 36.88 to 31.69 mmol C g^{-1}) and O (from 28.44 to 24.35 mmol O g^{-1}) elements, despite the presence of long hydrocarbon chains (i.e., 2 propyl groups) and 3 O moieties in DBCHPP. Obviously, the clearer marker of chemical modification is given by P-content: phosphorus element appears in the functionalized material with a content of 12.44 % (*w*/w), corresponding to 4.02 mmol P g^{-1} in GEG-P. It is noteworthy that chlorine appears in the sorbent at non-negligible levels (0.085 and 0.181 mmol Cl g^{-1}); this may be attributed to the presence of impurities or incomplete substitution of DBCHPP onto EPI backbone. Based on the supposed structure of gellan gum equivalent molecular unit (constituted of 2 β-D-glucose residues, 1 β-L-rhamnose residue, and 1 α-D-glucuronic acid residue), and the analytical data it is possible calculating the approximate substitution yields:

(a) 0.054–0.066 mmole TSCZ per GEG unit in GEG-C (calculations made on S and N contents, respectively), and.
(b) about 0.72 mmol DBCHPP per GEG unit in GEG-P (calculations made on P content).

Fig. S4 shows the titration of sorbents (pH-drift method) for the determination of the pH of zero charge (pH_{PZC}). The thiosemicarbazide-derivative of GEG shows a pH_{PZC} value close to 6.26. This is strictly different than the behavior reported by Fasolin et al. [73]: the zeta potential of GG remains negative in the pH 3–7 region, consistently with their evaluation of the pK_a of low-acyl GG, close to 3.5. Cassanelli et al. [74] confirmed this trend with another electrophoretic mobility method. The pK_as values of the reactive groups on thiosemicarbazide range between 1 (for the strongest acid group) and 14.76 (for the strongest basic group). After grafting onto GEG, the amine groups (i.e., 3 amine moieties) on TSCZ contribute to partially "neutralize" the proper acidity of the biopolymer. Based, on the low density of TSCZ in GEG-C, this effect is relatively limited. On the other hand, after grafting the organophosphate substituent the pH_{PZC} shifts toward lower value: 5.45. The organophosphate compounds (such as mono- and di-butyl phosphate) have acid pK_a values around 1.80–1.72 [75]. Therefore, the derivative of TBP grafted onto the sorbent shifts the pH_{PZC} of GEG-P toward slightly lower value. The functionalization of GEG-C allows getting a sorbent negatively charged at lower pH; this may have a weak impact on the electrostatic attraction of positively charged metal ions.

3.2. Sorption from synthetic solutions

3.2.1. pH effect

The effect of the pH on Cd(II) sorption by GEG-C and GEG-P sorbents is presented in Fig. 2, at two temperatures (i.e., T: 21 ± 1 °C and T: 50 ± 1 °C). This figure shows that:

(a) the sorption capacity is negligible at pH_0 1 and comparable for the two sorbents (q_{eq}: 0.12–0.15 mmol Cd g^{-1}),
(b) the sorption increases with the pH; more steeply for GEG-P, compared with GEG-C, consistently with the acid-base properties of the sorbents (pH_{PZC} values),
(c) the sorption capacity tends to stabilize at $pH_{eq} > 5$,

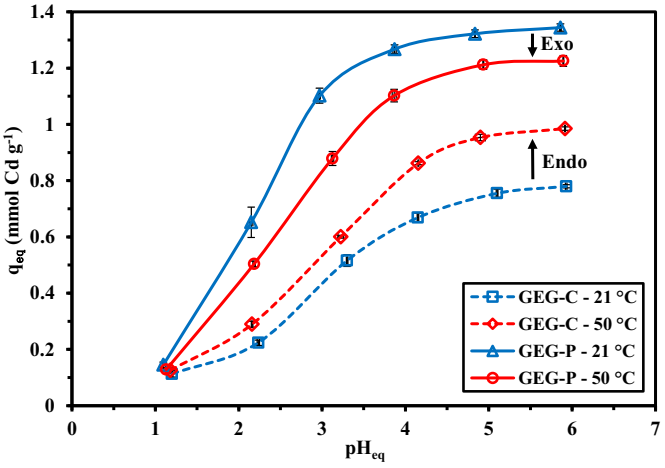

Fig. 2. Effect of pH and temperature (21 ± 1 °C and 50 ± 1 °C) on Cd(II) sorption using GEG-C and GEG-P sorbents (C_0: 0.953 mmol Cd L^{-1}; Sorbent dose, SD: 0.667 g L^{-1}; time: 48 h; v: 210 rpm).

(d) the functionalization of the GEG-C sorbent significantly increases sorption capacity (from 0.78 mmol Cd g^{-1} to 1.34 mmol Cd g^{-1}; +72 %),

(e) the increase in the temperature has opposite effects for the two sorbents: Cd(II) sorption is exothermic for GEG-P, while the sorption is endothermic in the case of GEG-C. Increasing the temperature minimizes the difference in sorption capacity (0.99 mmol Cd g^{-1} for GEG-C and 1.23 mmol Cd g^{-1}; +24 %, instead of +72 %),

(f) further experiments will be performed at pH_0 5; except for the study of selectivity issues, to evaluate the possibility to increase the separation of cadmium from competitor ions on the basis of pH criterion.

In acidic solutions, (i.e., pH 1), the protonation of reactive groups limits the possibility to bind cadmium cations by electrostatic repulsion and competition of protons. Fig. S5 shows the speciation diagram of cadmium (under the experimental conditions of the study of pH effect). Cadmium cations (predominant $CdCl^+$ and free Cd^{2+}) represent 81.5 % of total cadmium. The limited sorption capacity may be explained by the ion-exchange of these cationic species with protons bound to reactive groups, and/or the chelation of neutral $CdCl_2$. At pH 2, free Cd^{2+} begins to predominate and the sorption capacity increases; especially for GEG-P: the higher density of reactive groups due to the grafting of TBP-derivative may explain this stronger increase. This effect may be also reinforced by the impact of lower pH_{PZC} (deprotonation of reactive groups is facilitated). The increase in sorption capacity is almost linear for GEG-P between pH_0 1 and 3–4 (at both T: 21 ± 1 °C and T: 50 ± 1 °C). At pH_0 4, the sorption capacity continues to increase but moderately. It is noteworthy that this pH "frontier" corresponds to the region where the distribution of Cd(II) between free Cd^{2+} and $CdCl^+$ tends to stabilize (around 87 % and 13 %, respectively, at pH 4). It is also noticeable that this pH region corresponds to the deprotonation of carboxylic groups and amine groups; despite the favorable deprotonation conditions, the sorption is not significantly enhanced. The diminution in the competition of protons may help in binding cadmium cations through ion-exchange with partially protonated reactive groups (carboxylate and amine groups in both GEG-C and GEG-P) and the chelation of the metal with phosphate moieties (in the case of GEG-P). Under mild acidic conditions, the tautomerization effect activates the thiocarbonyl groups with neighboring amines (observed through the changes on FTIR spectra), which contribute to metal binding.

It is noteworthy that cadmium sorption is exothermic for GEG-P and endothermic for GEG-C. In contrast, Mellah and Benachour [76] reported that cadmium extraction by TBP (in solvent extraction system) is endothermic. The inversion of the effect of temperature on the pH-profile of Cd(II) sorption may be associated with opposite thermodynamic behavior of functional groups (amine groups for GEG-C vs. phosphate and thiocarbonyl groups for GEG-P) in their interactions with Cd(II). Complementary extensive study would be necessary for ascertaining this hypothesis.

Fig. S6 shows that the pH weakly varies during metal sorption. At pH below 4, the equilibrium pH slightly increases; reversely, above pH 4, the pH tends to decrease (at least for GEG-P, less for GEG-C). However, the variations remain systematically below 0.5 pH unit. Contrary to other metal ion systems, cadmium does not form hydrolyzed species (below 0.2 %) on the whole investigated pH range; therefore, the contribution of the formation of these species (with consumption of $-OH^-$) is negligible. On the other hand, the binding of protons (at pH below 4) hardly changes the pH. In Fig. S7, the $\log_{10}$ plot of the distribution ratio (i.e., D, L g^{-1}) vs. equilibrium pH does not show linear trends. This plot is usually applied for the determination of the stoichiometric exchange ratio in ion-exchange systems. The non-linearity supports the hypothesis of mixed mechanisms involving different modes of interactions such as chelation, in addition to ion exchange.

3.2.2. *Uptake kinetics*

The comparison of Cd(II) kinetic profiles in Fig. 3 confirms that the functionalization of GEG-C improves the sorption performance not only in terms of equilibrium (lower residual concentration and consequently higher sorption capacity) but also taking into account kinetic criterion. Indeed, 30 min are sufficient for reaching the equilibrium with GEG-P, while it is necessary extending the contact time up to 60 min for GEG-C. The steepest initial slope of the curve for the functionalized material (all other conditions being similar) also demonstrates this enhanced kinetic behavior. Since, the textural properties are very close for the two sorbents, it is probable that the stronger affinity (and greater density) of the reactive groups for cadmium explains this faster sorption: the diffusional restrictions are not playing the major role in the differentiation of the two sorbents in terms of kinetics.

The kinetics of sorption of may be controlled by different mechanisms of resistance to diffusion (diffusion in the bulk of the solution, through the film surrounding the particles, or into the porous internal network) [59]. The kinetics may be also simulated with classical equations derived from the modeling of homogeneous chemical reactions (i.e., pseudo-first and pseudo-second order rate equations, Table S1). The comparison of the models (summarized in Table 1) clearly shows that the pseudo-first order rate equation (PFORE) fits better experimental profiles for the two sorbents (though the PFORE gives higher statistical values for GEG-P sorbent). In Fig. 3, the solid lines represent the superposition of fitted curves with experimental points, while Fig. S8 shows the poorer fits of profiles with the PSORE and the RIDE models

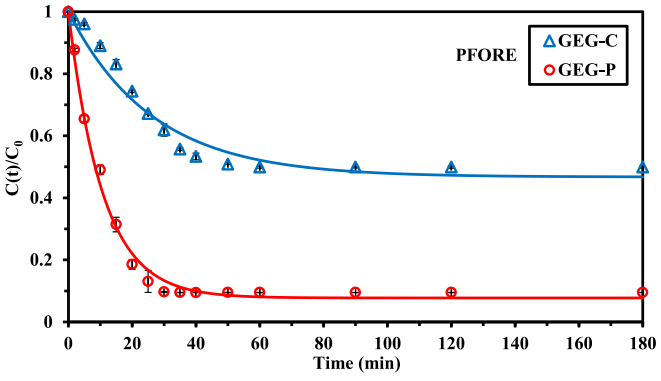

Fig. 3. Cd(II) uptake kinetics using GEG-C and GEG-P – Modeling with PFORE (pH_0: 5; C_0: 0.938 mmol Cd L^{-1}; SD: 0.66 g L^{-1}; T: 21 ± 1 °C; v: 210 rpm).

Table 1
Modeling of Cd(II) uptake kinetics for GEG-C and GEG-P sorbents.

Model	Parameter	Unit	GEG-C			GEG-P		
			#1	#2	Aver.	#1	#2	Aver.
Experimental	$q_{eq,exp}$	mmol Cd g^{-1}	0.729	0.686	0.712	1.31	1.26	1.29
PFORE	$q_{eq,1}$	mmol Cd g^{-1}	0.772	0.743	0.757	1.33	1.29	1.31
	$k_1 \times 10^2$	min^{-1}	3.78	3.83	3.81	8.82	9.86	9.33
	R^2	–	0.976	0.959	0.968	0.994	0.992	0.994
	AIC	–	−99	−90	−94	−107	−103	−106
PSORE	$q_{eq,2}$	mmol Cd g^{-1}	0.942	0.910	0.926	1.50	1.43	1.47
	$k_2 \times 10^2$	g $mmol^{-1}$ min^{-1}	4.17	4.31	4.24	8.16	9.69	8.89
	R^2	–	0.946	0.922	0.935	0.965	0.959	0.963
	AIC	–	−88	−81	−85	−80	−78	−79
RIDE	$D_e \times 10^{13}$	m^2 min^{-1}	1.38	1.43	1.40	0.425	0.483	0.452
	R^2		0.945	0.923	0.935	0.969	0.964	0.967
	AIC		−85	−80	−82	−78	−77	−78

(RIDE corresponds to resistance to intraparticle diffusion, herein approached with the Crank equation; See Table S1). It is noteworthy that the PFORE allows closer determinations of the equilibrium sorption capacities (compared with experimental values): the $q_{eq,1}$ overestimates the $q_{eq,exp}$ by 6 % for GEG-C and only 2 % for GEG-P. The faster sorption of Cd(II) using GEG-P is confirmed by the ≈2.45-fold increase of the apparent rate coefficient (i.e., k_1) with sorbent functionalization (from 0.0381 to 0.0933 min^{-1}). In the case of cadmium sorption onto chemically-modified brown alga biomass [77], the PSORE gave little better modeling than the PFORE, the apparent rate coefficient k_1 was lower (0.02 min^{-1}) than herein. In the case of electrospun PEO/chitosan nanofiber membranes, the apparent rate coefficient was also slightly lower (i.e., 0.028 min^{-1}) than for GEG-C sorbent [78]. Jakóbik-Kolon et al. [79] showed close fittings of kinetic profiles with PFORE and PSORE while using a series of polysaccharide composites: the k_1 values varied between 0.013 and 0.032 min^{-1}. These values are consistent with the value reported by Maki and Qasim [80] for Cd(II) sorption kinetics with KOH-activated peanut shells (i.e., 0.024 min^{-1}). In the case of magnetic chitosan microparticles functionalized with hydrazide, Hamza et al. [81] reported k_1 value (i.e., 0.076 min^{-1}) closer to the case of GEG-P.

Though the RIDE (resistance to intraparticle diffusion equation, the so-called Crank equation) does not fit kinetic profiles as well as PFORE (Fig. S8), the equation is used for approaching the effective diffusivity of Cd(II) into the sorbent (i.e., D_e). The diffusion coefficient is lower for GEG-P (≈0.45 × 10^{-13} m^2 min^{-1}) than for GEG-C (≈1.4 × 10^{-13} m^2 min^{-1}). The effective diffusivity is about 5 orders of magnitude lower than the free diffusivity of Cd(II) in water (D_0: 4.31 × 10^{-8} m^2 min^{-1}, [82]). This gap in the diffusivity coefficients (vs. free diffusivity in water) confirms that the resistance to intraparticle diffusion plays a significant part in the control of uptake kinetics. The global kinetic is controlled by the resistance to intraparticle diffusion and the proper reaction rate of sorption.

3.2.3. *Sorption isotherms*

The sorption isotherms represent the evolution of sorption capacity (i.e., q_{eq}) with residual concentration (i.e., C_{eq}). Herein, the sorption isotherms of GEG-C and GEG-P show differences in their profiles. In the case of reference sorbent (GEG-C) the sorption capacity progressively and continuously increases with metal concentration; apparently, in the last section of the curve (above C_{eq}: 3 mmol Cd L^{-1}) the sorbent is not saturated. On the opposite hand, the sorption isotherm for GEG-P shows a steep initial slope (almost vertical, corresponding to a quasi-irreversible isotherm) of the sorption capacity (at residual concentration below 0.2 mmol Cd L^{-1}), followed by a progressive increase in sorption capacity that tends to a saturation plateau for C_{eq} ≈ 2.5 mmol Cd g^{-1}. The effect of functionalization is also measured through the comparison of maximum (experimental) sorption capacity: the sorption capacity increases by 1.74-fold after grafting TBP-derivative. Cd(II) is classified among the borderline metals [83]. According to the hard and soft acid and base theory (HSAB, [84]), hard acid prefer reacting with hard bases, and reciprocally soft metals with soft bases. On the other side, sulfhydryl (-SH and more generally sulfur-based) is part of soft bases, amine groups (and more generally N-bearing ligands) take place in the intermediary class, while O-bearing ligands (such as carboxylate and phosphate groups) are considered hard bases. The increase in sorption capacities can be directly related with the enhanced density of reactive groups after functionalization. The case of affinity coefficient (which is proportional to the initial slope of the curve) is more complex to discuss. Indeed, the strong increase in the initial slope means that GEG-P has a strong affinity for Cd(II); however, the new functional groups (bearing O-ligands; i.e., hard base) are supposed to show greater reactivity for hard metals than for intermediary metals (such as Cd(II)). Apparently, the increase in the density of reactive groups (associated with P content: 4 mmol P g^{-1}, Table S3) plays a major role in the enhancement of Cd(II) sorption rather than the proper affinity of reactive groups. This conclusion can be modulated by the synergistic effect brought by the dual functionalities [53].

Table 2
Modeling of Cd(II) sorption isotherms for GEG-C and GEG-P sorbents.

Model	Parameter	Unit	GEG-C	GEG-P
Experimental	$q_{m,exp}$	mmol Cd g^{-1}	1.60	2.79
Langmuir	$q_{m,L}$	mmol Cd g^{-1}	1.92	2.63
	b_L	L $mmol^{-1}$	1.24	21.1
	R^2	–	0.988	0.960
	AIC	–	−52	−29
Freundlich	k_F	$L^{1/nF}$ $mmol^{1-1/nF}$ g^{-1}	0.974	2.33
	n_F	–	2.33	3.91
	R^2	–	0.994	0.940
	AIC	–	−64	−24
Sips	$q_{m,S}$	mmol Cd g^{-1}	3.79	3.06
	b_S	$(L\ mmol^{-1})^{1/nS}$	0.363	4.49
	n_S	–	1.72	1.53
	R^2	–	0.997	0.973
	AIC	–	−67	−29
Temkin	A_T	L $mmol^{-1}$	42.0	385
	b_T*	kJ mol^{-1}	13.2	16.6
	R^2	–	0.961	0.981
	AIC	–	−43	−37
Dubinin-Radushkevich	$K_{DR} \times 10^9$	mol^2 J^{-2}	5.05	2.57
	E_{DR}	kJ mol^{-1}	14.0	19.7
	R^2	–	0.997	0.960
	AIC	–	−70	−28
Langmuir dual site	$q_{m,1}$	mmol Cd g^{-1}	0.416	1.93
	b_1	L $mmol^{-1}$	17.8	39.5
	$q_{m,2}$	mmol Cd g^{-1}	2.00	1.48
	b_2	L $mmol^{-1}$	0.437	0.591
	R^2	–	0.998	0.982
	AIC	–	−66	−28

Modeling on the averaged points of duplicated series.

Table 2 summarizes the fits of sorption isotherms with a series of classical models (which are reported in Table S2). Based on the profiles in Fig. 4, it is possible anticipating that GEG-C and GEG-P could follow different trends. Indeed, GEG-P is characterized by a saturation plateau, which makes the power-type function of the Freundlich equation inappropriate, contrary to GEG-C (characterized by an exponential trend). Actually, the saturation is not reached in the concentration range; this probably means that the distribution of experimental points forces the fit of experimental profile with the Freundlich equation. The Freundlich equation supposes the sorption to occur in a multi-layer mode with possible interactions between sorbed molecules (with heterogeneous sorption energies). The mechanistic Langmuir equation is associated with homogeneous monolayer sorption (without interactions between sorbed molecules). This equation supposes an asymptotic trend, which is consistent with the profile of GEG-P curve: the Langmuir equation fits better the curve than the Freundlich equation. The Sips equation combines the Langmuir and Freundlich equations. In the Langmuir Dual Site equation, the Langmuir model is applied independently for two different sorption sites (having different sorption capacities and affinity coefficients). The Temkin model assumes a uniform distribution of heterogeneous sorption sites and a binding energy that varies linearly with surface coverage [61]. The Dubinin-Radushkevich equation was developed for describing sorption at the surface of microporous sorbents (micropore volume fitting processing through layer-by-layer adsorption on pore walls) [62]. Several works alerted on the debatable appropriateness of interpreting binding mechanisms on the basis of mathematical fits of experimental profiles. Many of these misinterpretations are related to the wrong extension of the gas/solid equation (original concept) to liquid/solid systems. Hence Hu et al. [85] suggest using only these equations for comparative and predictive target.

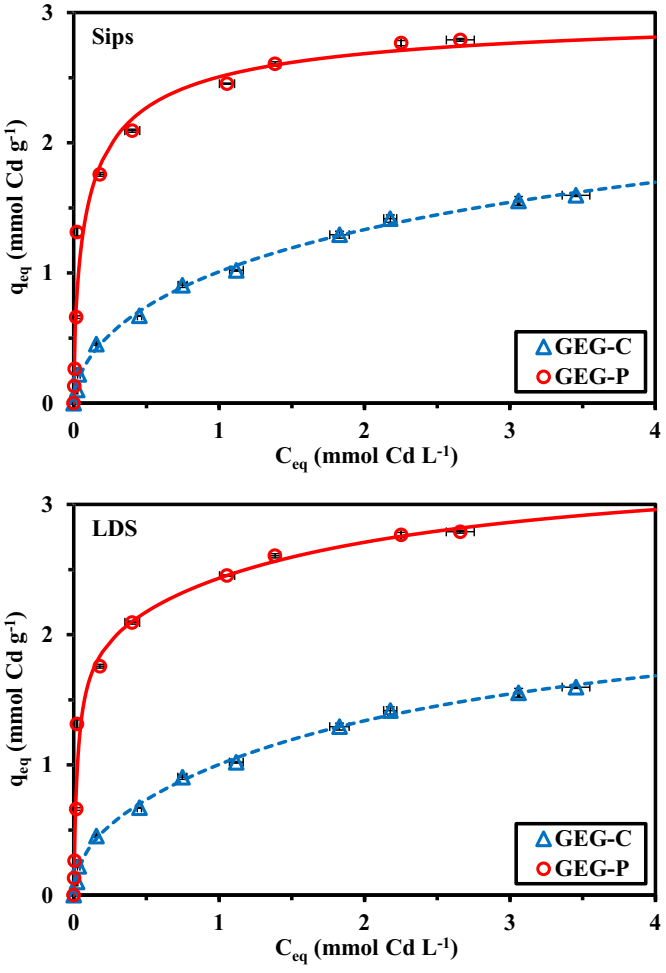

Fig. 4. Cd(II) sorption isotherm using GEG-C and GEG-P – Modeling with the Sips equation and the Langmuir Dual Site equation (pH_0: 5; C_0: 0.088–4.52 mmol Cd L^{-1}; SD: 0.667 g L^{-1}; T: 21 ± 1 °C; v: 210 rpm; time: 48 h).

Considering both R^2 and AIC statistical criteria, Table 2 shows that the preferential fits follow different trends for the two sorbents:

GEG-C: D-R > Sips ≈ LDS > Freundlich ≫ Langmuir ≫ Temkin

GEG-P: Temkin ≫ Langmuir ≈ Sips ≈ D-R ≈ LDS ≫ Freundlich

In Fig. 4 the experimental profiles are fitted with the Sips and the Langmuir Dual Site equations (as the closer models for combined GEG-C and GEG-P sorbents), alternative fits are reported in Fig. S9. In order to compare Cd(II) sorption properties of GEG-C and GEG-P with other sorbents, the parameters of the Langmuir equation are used in Table S4 (because widely referred to in the literature). The sorption performances can be compared based on different criteria: the pH selected for optimum binding, the required time for reaching equilibrium, the maximum sorption capacity, and the affinity coefficient. Sorption tests are performed in most cases between pH 4 and pH 7 (meaning mild acidic or neutral conditions). A biosorbent (*Trichoderma atrobrunneum*) shows high sorption capacity (3.07 mmol Cd g^{-1}); however, the interest is limited by slow kinetics (requiring up to 7 days of contact for reaching the equilibrium) [86]. GEG-P shows excellent sorption characteristics for Cd(II), comparable to the best sorbents such as C-150 sulfonic resin [87], Amberlite IR-120 (sulfonic resin) [88], 3-D sulfonated reduced graphene oxide [89], nitrilotriacetic acid/magnetic Prussian blue [90], or $MnFe_2O_4$/Graphene oxide [91]. Sorption capacities range between 2 and 2.5 mmol Cd g^{-1} with equilibrium times below 180 min. The affinity coefficient of GEG-P are comparable to those of these outstanding sorbents, except for nitrilotriacetic acid/magnetic Prussian blue [90] or $MnFe_2O_4$/Graphene oxide [91] that show b_L coefficients about 6-fold higher than the value of GEG-P. However, taking into account the combination of the different criteria, GEG-P can be considered a highly competitive and promising sorbent.

3.2.4. *Sorption mechanisms*

The FTIR analysis the sorbents exposed to Cd(II) solutions have confirmed the modification of the chemical environment of carboxyl, amine and thiocarbonyl groups in the case of GEG-C at pH_0 5 (where Cd^{2+} predominates, in addition to 12 % of $CdCl^+$). The interactions probably involve electrostatic attraction of cadmium cations (free Cd^{2+}) onto carboxylate sites (free groups), ion-exchange mechanism between Cd^{2+} (or $CdCl^+$) and some protonated amine groups, and chelation mechanism between amine and thiocarbonyl groups with cadmium ions. In the case of GEG-P, the FTIR analysis also showed the modification of the signals associated with phosphate moieties (from TBP derivative). This chemical modification also shifted the pH_{PZC} of the sorbent toward lower value; meaning that more amine groups are potentially deprotonated (modulating the contribution of ion exchange and chelation contributions). In addition, to the mechanisms involved in Cd(II) binding onto GEC-C, cadmium can be also chelated onto phosphate moieties. As reported in the comparison of pH effect for GEG-C and GEG-P (in Section 3.1.5.), the differences in the pH_{PZC} values lead, for a given pH, that the surface of the functionalized sorbent is more negatively charged than for GEG-C. This results in a stronger binding of cadmium. Scheme 2 illustrates the different mechanisms involved in metal binding.

3.2.5. *Metal desorption and sorbent recycling*

Another important criterion in the evaluation of a new sorbent concerns (a) the ability to eluate bound metal, and (b) the capacity to recycle the sorbent. Though some complexing agent (such as 0.1 M EDTA solution) have been tested for Cd(II) desorption from saturated biosorbent such as chitosan – κ-carrageenan composite [92], acidic solutions are most frequently used. For commercial resins, Taha et al. [93] used 1 M acid solutions (with limited effect of the type of acid). In the case of bio-sourced sorbents (simple or composite) moderate acid

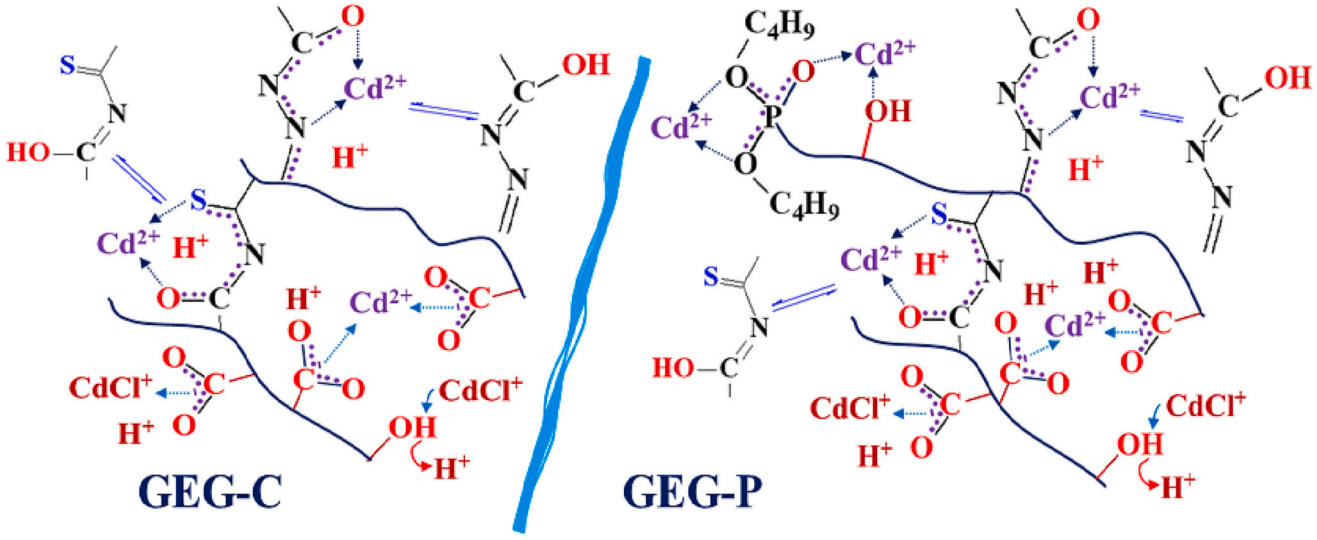

Scheme 2. Tentative mechanisms for Cd(II) sorption onto GEG-C and GEG-P sorbents.

solutions (0.1–0.5 M) were preferred using either nitric acid solutions [94,95] or hydrochloric acid solutions [81,96,97]. Apart the literature information, the strong reduction in sorption capacity observed at low pH is another incentive for using an acid solution. Hereafter, 0.3 M HCl solution is used for the desorption of Cd(II) from metal-loaded sorbents. Fig. S10 compares the kinetics of desorption for Cd(II)-loaded GEG-C and GEG-P sorbents (loaded samples collected from the study of uptake kinetics). The desorption kinetics are comparable for the two sorbents; though cadmium tends to be released lightly faster for GEG-P material. In any case, total desorption is achieved in <30 min. Jakobik-Kolon et al. [94] also reached quantitative desorption of Cd(II) from pectin-guar gum sorbent using 0.25 M HNO_3 solution.

Based on these results, 0.3 M HCl solution was selected for testing the recycling of the sorbent. Demineralized water solutions were used between each step for rinsing the sorbent to remove both absorbed cadmium solution and HCl solution. Table 3 compares the sorption and desorption performances for five successive cycles of reuse. Metal desorption remains effective and complete for the five cycles. On the other hand, a weak decrease in sorption efficiency is observed at recycling. In the case of GEG-C, the loss in sorption efficiency between the first and the fifth step reaches about 4.6 %. This is detectable but relatively limited. This is consistent with the stability observed in the FTIR spectrum (Section 3.1.4., where the spectra are compared for raw sorbent and recycled material). It is noteworthy that in the case of GEG-P, the loss at the fifth cycle does not exceed 1.8 %. The functionalization of the material notably increases the stability in sorption performance. In the case of nano-composite magnetic attapulgite functionalized with chitosan and EDTA, Wang et al. [97] reported a decrease in the sorption efficiency of about 10 % (from 98.9 % to 88.7 % at the fifth cycle).

The grafting of TBP derivative onto GEG-C allows reinforcing the stability in sorption performance during sorbent recycling. Combined with the other enhancement on sorption capacities and uptake kinetics; this result confirms the promising perspectives opened by this material.

Table 3
Sorbent recycling – Sorption and desorption efficiencies (SE and DE,%, respectively).

Cycle	GEG-C		GEG-P	
	SE (%)	DE (%)	SE (%)	DE (%)
1	50.7 ± 0.2	100.2 ± 0.3	96.6 ± 0.5	100.3 ± 0.4
2	50.1 ± 0.3	99.8 ± 0.8	96.1 ± 0.2	99.9 ± 0.1
3	49.5 ± 0.3	99.9 ± 0.1	95.6 ± 0.3	99.9 ± 0.2
4	48.9 ± 0.6	100.1 ± 0.1	95.3 ± 0.5	100.3 ± 0.1
5	48.4 ± 0.8	100.1 ± 0.3	94.9 ± 0.2	100.3 ± 0.4
Loss at 5th cycle	4.6 %	Negligible	1.8 %	Negligible

3.2.6. *Selectivity – sorption from multi-component solutions*

The selectivity for specific metal ions is another key criterion in the design of new sorbents. The grafting of new reactive groups with specific reactivity, their steric and cooperative arrangement (for accommodating chelation sphere) may contribute to change the preference of the sorbent for different metal families based on softness, ion size, charge, electronegativity, and so on [98].

For both GEG-C and GEG-P, cadmium is preferentially sorbed against the other metal ions, as shown in Fig. 5, where the selectivity coefficient $SC_{Cd/metal}$ is plotted for different pH values. In most cases, the selectivity increases with the pH. It is noteworthy that at the lowest pH value (i.e., $pH_{eq} \approx 2.2$), the selectivity for Cd(II) is lost, especially for GEG-P, where apparently the sorbent binds preferentially the other metal cations. The protonation of reactive groups exhibits lower effect on their sorption than on Cd(II) uptake. On the reverse side, when the pH increases the progressive deprotonation increases the preference of GEG-C for Cd(II); this effect is sharply marked between pH_{eq} 2.14 and pH_{eq} 4.17, while above the effects tends to stabilize.

It is noteworthy that the sorbents have similar responses in terms of selectivity for Cd(II) (Fig. 5) and Pb(II) (Fig. S11); though the sorbents have marked preference for Cd(II) over Pb(II), these metal ions showed much larger differences against other competitor metals. This behavior can be correlated with their HSAB ranking. Nieboer and Richardson [83] displayed the distribution of the metal ions according their position in the plot "covalent index" ($CI = \chi^2 \times r$; where χ is the Pauling electronegativity and r the radius of hydrated ion) vs. "ionic index" ($II = z^2/r$, where z is the formal charge of the metal ion). Lead(II) and cadmium(II) are located in the upper part of the borderline metal ions while zinc(II) and iron(III) are closer from the frontier with class A metals (hard acids). Other competitor ions (i.e., Al(III), Mg(II), Ca(II), and Na(I)) are classified among the hard metal ions. According HSAB principle [84], hard acids react preferentially with hard bases, following the ligand scale O > N > S. For soft acids (class B), the preference is reversed: S > N > O. The discussion is more complex for borderline elements. The interpretation is made complex by the variations induced by pH changes. Hence, in mildly acidic conditions a borderline metal ion binds to O-bearing ligand (such as carboxylate moiety) preferentially to amine groups, while these amine groups require to be deprotonated (higher pH, close to neutral) for actively binding the borderline metal ion [83]. Considering the highest SC values (in the pH_0 range ≥ 4), the metal ions can be ranked in

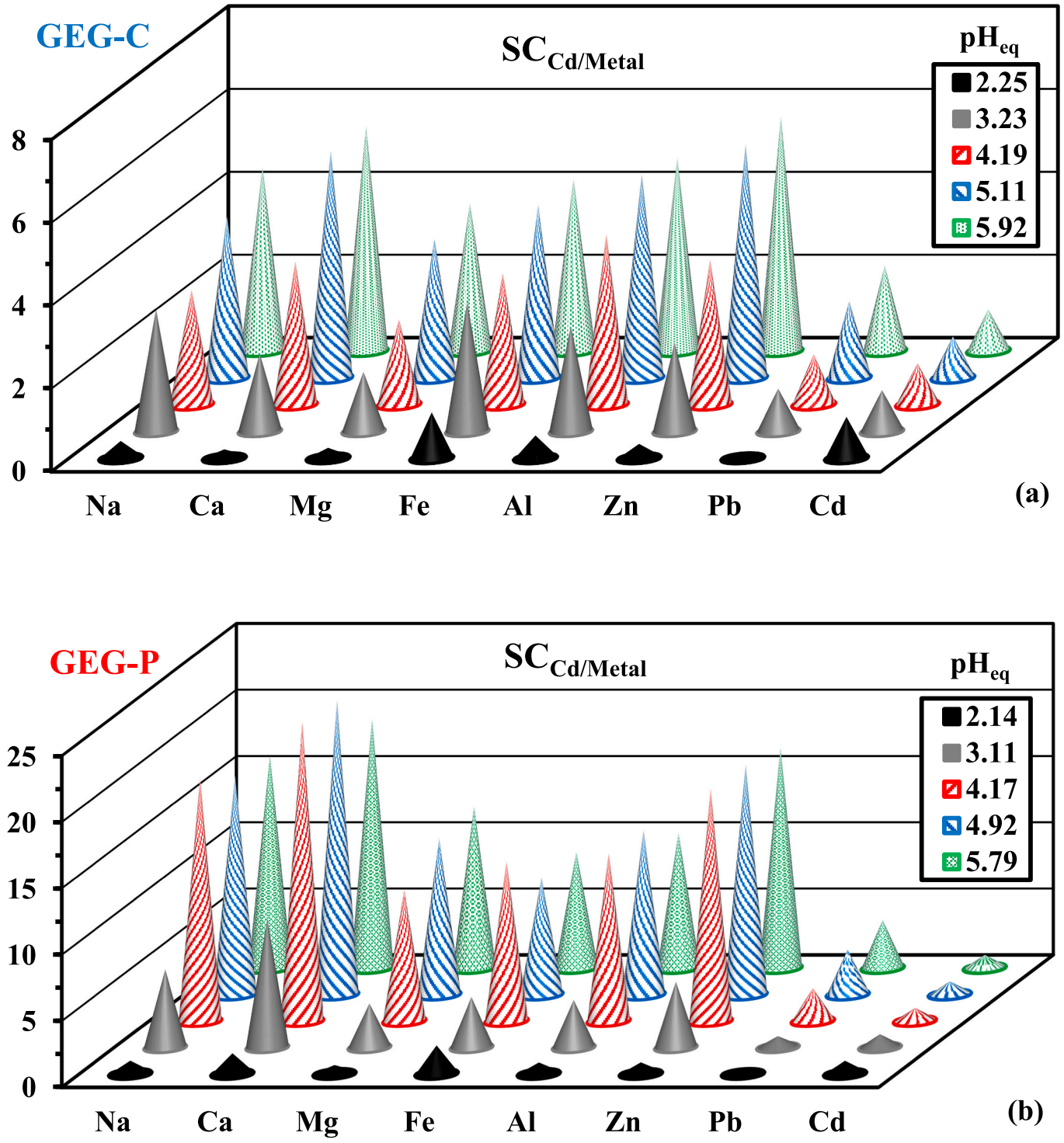

Fig. 5. Effect of pH_{eq} on the $SC_{Cd/metal}$ for GEG-C (a) and GEG-P (b) (multicomponent equimolar solutions, C_0: 1 mmol L^{-1}; SD: 1.0 g L^{-1}; v: 210 rpm; T: 21 ± 1 °C; time: 24 h; $SC_{Cd/Cd} = 1$ as reference).

terms of increasing preference for Cd(II) according the series:

$$\text{For GEG} - \text{C } (pH_0 \geq 5) : \text{Pb(II)} \ll \text{Fe(III)} \approx \text{Mg(II)} \approx \text{Al(III)} < \text{Zn(II)} < \text{Na(I)} \ll \text{Ca(II)} \quad (2)$$

$$\text{For GEG} - \text{P } (pH_0 \geq 4) : \text{Pb(II)} < \text{Mg(II)} < \text{Fe(III)} < \text{Na(I)} < \text{Al(III)} < \text{Ca(II)} < \text{Zn(II)} \quad (3)$$

In the case of Dowex AG50W-X8 (sulfonate-bearing resin, strongly acidic cation exchange resin) [99]: the selectivity order followed the series:

$$\text{Na(I)} < \text{Mn(II)}, \text{Mg(II)} < \text{Fe(III)} < \text{Cd(II)}, \text{Zn(II)} < \text{Cu(II)} < \text{Ca(II)} < \text{Al(III)} \quad (4)$$

The selectivity may be modulated by the pH through different mechanisms associated with metal speciation (formation of hydrolyzed species) and with the deprotonation of reactive groups (amine, phosphate, carboxylic groups), which, in turn, may vary the relative

contributions of different binding mechanisms (chelation vs. ion-exchange) [100]. With the deprotonation of the reactive groups, the chelation mechanisms are stimulated bringing differentiated affinity for target metals (based on HSAB principles).

Alexandratos and Zhu [52] discussed the selectivity of a series of monophosphorylated polymer supported reagents for divalent and trivalent cations. In the case of divalent cations, they showed that the distribution ratios are linearly correlated with the Misono softness parameter [101]; meaning that the metal ions form dative π bonds with the ligand (single-site interaction). In the current study, these trends were not respected; this is probably due to the interaction of vicinal reactive groups that interfere on the polarizability properties of phosphate moieties. More specifically, they consider that divalent cations may bind to the polarizable phosphoryl oxygen [101], while the greater charge of trivalent metal ions brings closer the solute to phosphoryl oxygen, which, in turn, allows binding the trivalent cations with both the phosphate and –OH moieties. Elsayed et al. [102] documented the synthesis of ion-imprinted sorbents based on thiosemicarbazide/salicylic acid/Cd(II) complex immobilized in resorcinol/formaldehyde resin. The ion-imprinting drastically increased the distribution ratio for Cd(II) (up to 612 L g^{-1} at pH 6), and the selectivity coefficient $SC_{Cd/metal}$ was multiplied by a factor 20–22 compared to non-imprinted resin (against metal ions with close valence and ionic size: Pb(II), Cu(II), Zn (II), and Ni(II)). The imprinting strategy was also applied by Murat et al. [103] for enhancing (by a factor 3.3–3.9) the selectivity of maleic acid-*co*-acrylonitrile sorbent for Cd(II) against Pb(II), Mn(II), Ni(II), and Cu (II). Hu et al. [104] synthesized aerogels with self-assembly nanosheets (made of salecan, a water-soluble anionic extracellular glucan, and graphene oxide) for the sorption of Cd(II). The sorbent showed preference for Cd(II) against a series of transition metals: the distribution ratio did not exceed 0.63 L g^{-1} remaining greater than for:

$$Co(II) > Ni(II) > Zn(II) > Cu(II) > Hg(II) > Pb(II) > Fe(III) \quad (5)$$

However, both the extraction and selectivity for Cd(II) were considerably increased after ion-imprinting: the selectivity ratio increased up to 6.4 L g^{-1} and the $SC_{Cd/metal}$ value was increased by 13-fold to 84-fold.

Fig. S12 plots the $\log_{10}$ plot of the distribution ratio vs. pH_{eq} for the two sorbents and selected metal ions. As reported above, the increase of the pH increases the distribution ratios up to pH_{eq} 4.2–5, before stabilizing. The distinct behavior of Cd(II) and Pb(II) is clearly highlighted by this plot. The gap between these two metal ions (especially Cd(II)) and other competitor elements is drastically increased with the functionalization of the sorbent (phosphate moieties from TBP derivative).

These rankings can be visualized in Fig. S13 (CI vs. II plot frame); the size of the bubbles for the distinct elements is proportional to the distribution ratio (normalized against cadmium as the most favorably sorbed metal). The preference of the sorbents for Cd(II) and Pb(II) means that their reactive groups have higher affinity for borderline elements (with higher CI values). GEG-P shows much lower affinity for the hard metals (such as Na(I), Ca(II), and Mg(II)) (despite the presence of hard base reactive groups, brought by TBP derivative); this contrasts with the lower selectivity of GEG-C for the hard acids. Considering Fe(III) and Al (III) trivalent metal ions (located at the interface between borderline and hard acids), the trends are comparable to the observations made with hard metals: the distribution ratios are also substantially decreased in the case of GEG-P (compared with GEG-C). The case of Zn(II) (ranked among borderline elements close to Cd(II)) also shows much lower relative distribution ratio in the case of GEG-P. The trends in (Eq. (2)) and (Eq. (3)) regarding Zn(II) ranking clearly demonstrate that this metal ion leaves the expected projections. This is consistent with the restrictions introduced by the Irving-Willians series [105]: Zn(II) remains out of the trend.

Table S5 summarizes the conditions (especially pH) for optimizing the separation of Cd(II) from the specific competitor metals for the two sorbent. In addition, the enhancement factor in the selectivity due to the functionalization of the sorbent is reported for these optimized conditions. The full plot of the enhancement factor of selectivity coefficient ($SC_{Cd/metal}$) is reported in Fig. S14 for the different pH_0 values.

The cumulative sorption capacities are summarized in Fig. S15. The trends on pH-edge curves are consistent with the profiles reported in Fig. 2 (mono-component Cd(II) solutions). At pH around 5, the cumulative sorption capacities are close to 1.32 mmol g^{-1} and 2.02 mmol g^{-1} for GEG-C and GEG-P sorbents, respectively (53 % increase in cumulative sorption capacity after functionalization, vs. +74 % with mono-component Cd(II) solutions). These values are systematically lower (by 17.5–27.6 %) than the maximum experimental values obtained from sorption isotherms at pH_0 5 (Fig. 4 and Table 2): 1.60 and 2.79 mmol Cd g^{-1}, respectively. The presence of competitor metal ions reduces the global sorption capacity of the sorbents. This means that the antagonistic effect of competitor metal ions decreases the global sorption potential.

3.3. Application to real effluent

The composition of the mining effluent is reported in Table 4. Cadmium and lead are present at low level (around 1 mg L^{-1}), while the concentration of other base metals (i.e., copper, zinc, iron and aluminum) ranges between 9 and 28 mg L^{-1}. These levels are much lower than for calcium (about 216 mg L^{-1}) and more specifically sodium (>2 g L^{-1}). This means that competitor ions are in large excess compared to the most toxic elements (cadmium and lead): from about 15-fold for iron and copper, 40-fold for aluminum and zinc and up to 520-fold for calcium and 8576-fold for sodium. After contact with GEG-C (under optimal pH selection; i.e., pH_0 5.83), the residual concentrations are strongly decreased for heavy metals with sorption efficiencies ranging between 27 and 32 % for Al and Zn, 46–49 % for Cd and Pb, and around 81 % for Cu and Fe (sorption of calcium and sodium remains below 17 %). These levels of sorption efficiency are controlled by the affinity of the sorbent for the metal ions but this effect is also strongly affected by the impact of initial concentrations. The concentration factor (CF, L g^{-1}) can be ranked according:

$$Fe > Cu \gg Cd > Pb \gg Zn > Al \gg Ca \gg Na \quad (6)$$

The comparison of residual concentrations with maximum concentration levels for drinking water [1] shows that the experimental conditions are not appropriate for the removal of the heavy metals (for copper the residual concentration is close to target values): the excess levels reach values as high as ~200 times for Cd and ~ 105 times for Pb. This test with complex solution clearly shows that GEG-C cannot be used at given sorbent dose (i.e., 1.5 g L^{-1}) for decontaminating the effluent.

The functionalization of the material with TBP-derivative strongly changes the treatment pattern. The residual concentrations are drastically reduced: 8–9 μg L^{-1} for Cd and Pb, 0.11–0.57 mg L^{-1} for Fe and Al, and 1.2–3 mg L^{-1} for Cu and Zn. This is confirmed by the sorption efficiencies that are systematically higher than 88.5 % for heavy metals, and up to 99.2 % for lead and cadmium. On the opposite hand, the functionalization does not significantly affect the removal of sodium and calcium; this is positive for the selective separation of target hazardous metal ions from alkaline and alkaline-earth metals. The concentration factors for heavy metals are systematically increased, following the order:

$$Cd, Pb, Fe > Al > Zn, Cu \gg Ca \gg Na \quad (7)$$

With GEG-P, the residual concentrations are compatible with drinking water regulations in the case of copper, zinc, iron; however, for cadmium, lead, and aluminum the residual concentrations remain about 1.5 to 3 times higher than imposed by regulations for drinking water. The treatment of the effluent with GEG-P (under selected experimental conditions) allows reaching the levels required for irrigation water (as defined by FAO); except for copper and zinc [106]. In Table 4, the comparison of the CFs for GEG-C and GEG-P allows calculating the

Table 4
Composition of the mining effluent and treatment criteria at optimum pH_0: 5.83 (equilibrium concentration, mg L^{-1} and mmol L^{-1}; Sorption efficiency, SE (%); Concentration factor, CF; and Enhancement factor due to functionalization, EF).

Metal	Na	Ca	Cu	Zn	Cd	Pb	Fe	Al
Conc. (mg L^{-1})	2043	215.9	10.56	27.55	1.165	0.968	9.065	11.60
Conc. (mmol L^{-1})	88.88	5.386	0.1662	0.4214	0.0104	0.00467	0.1623	0.4299
Molar ratio (metal/Cd)	8576	519.7	16.04	40.66	1	0.4508	15.66	41.49
C_{eq} (mg L^{-1}) for GEG-C	1859	179.0	2.16	18.63	0.596	0.523	1.55	8.43
C_{eq} (mg L^{-1}) for GEG-P	1908	171.0	1.22	3.05	0.009	0.008	0.11	0.569
$MCL_{d.w.}$ (mg L^{-1})	–	–	2.0	5.0	0.003	0.005	0.3	0.2
$MCL_{irrig..}$ (mg L^{-1})			0.2	2.0	0.01	5.0	5.0	5.0
SE (%) for GEG-C	9.03	17.1	79.6	32.4	48.8	46.0	82.9	27.3
SE (%) for GEG-P	6.64	20.8	88.5	88.9	99.2	99.2	98.8	95.1
CF for GEG-C	0.060	0.114	0.531	0.216	0.326	0.306	0.553	0.182
CF for GEG-P	0.044	0.139	0.590	0.593	0.662	0.661	0.659	0.634
EF	0.735	1.22	1.11	2.75	2.03	2.16	1.19	3.48

$MCL_{d.w.}$: Maximum concentration limit for drinking water, mg L^{-1}; $MCL_{irrig.}$: Maximum concentration limit for irrigation water (FAO, [106]), mg L^{-1}; SE: Sorption efficiency, %; CF: Concentration factor, q_{eq}/C_0, L g^{-1}; and EF: Enhancement factor, $F = \frac{CF_{GEG-P}}{CF_{GEG-C}}$, dimensionless.

enhancement factor brought in the removal of target metals by the functionalization of the pristine sorbent. The enhancement effect decreases according the order (Fig. S16):

$$Al \gg Zn \gg Pb, Cd \gg Ca, Fe > Cu \gg Na \quad (8)$$

Fig. S17 compares the selectivity coefficients $SC_{Cd/metal}$ (in function of pH) for GEG-C and GEG-P sorbents applied to the treatment of mining effluent. In most cases, the selectivity for target metal increases with the pH, due to the deprotonation of reactive groups at the surface of the sorbents. The concentration levels of the metals (with large excess of Na^+ and Ca^{2+}) may explain that the SC values (based on the relevant distribution ratio, which is strongly influenced by initial metal concentration) for calcium and sodium are much higher than for heavy metals. It is noteworthy that the functionalized sorbent exhibits considerably high $SC_{Cd/metal}$ values against calcium (about 489) and sodium (at 1806) at the most favorable pH (i.e., pH_0 5.89).

solution (based on their deprotonation for metal chelation or through ion-exchange properties with labile protons). However, the grafting of a derivative of tributylphosphate (DBCHPP) allows considerably enhancing sorption properties of the functionalized material (GEG-P): metal sorption occurs fastly; the sorption capacity and the affinity coefficient are both increased after chemical modification. The maximum sorption capacity of GEG-P sorbent (close to 2.79 mmol Cd g^{-1}) classifies the sorbent as one of the most efficient sorbents for this metal ion. Based on the study of pH effect at two temperatures, the sorption of cadmium is endothermic for GEG-C while it becomes exothermic for functionalized sorbent. Although the two materials are completely desorbed using 0.3 M HCl solution, the desorption kinetics is slightly faster for GEG-P sorbent; the recycling negligibly affects the stability of sorption performances: the loss in sorption properties decreases from 4.6 % to 1.8 % (at the fifth cycle). This improvement in sorption properties is also noticeable when comparing the selectivity coefficient for Cd(II) against other

$$\text{For GEG} - \text{C} : Na(9.6) \gg Ca(4.6) \rangle Al(3.0) \gg Zn(2.0) \gg Pb, Cd(1.0–1.1) \gg Cu, Fe(0.24–0.0) \quad (9)$$

$$\text{For GEGP} : Na(1806) \ggg Ca(489) \ggg Cu, Zn(16.7–16.0) \gg Al(6.6) \gg Fe(1.6) \rangle Pb(1.1) \quad (10)$$

It is noteworthy that the beneficial effect of the grafting of TBP-derivative cannot be directly correlated with the ranking of the metals within hard, intermediary, and soft classes. Hence, the major impact appears for aluminum (member of class A – hard acids), while the lowest effect is also observed for another member of hard acid metals (i.e., sodium). For the other heavy metal ions, the ranking in the enhancement factor does not follow clear trends against hydration enthalpy ($-\Delta G^0_{hydr.}$, kcal mol^{-1}), Ionic Index (II), Covalent Index (CI), or softness (σ, [82]) (Fig. S18). In the cases of the plots against the hydration enthalpy and the ionic index, the metal ions can be grouped first in function of their valence; within II group the respective ranking between the different metal ions cannot be correlated with specific physico-chemical criteria nor the positioning in the Nieboer and Richardson frame [83] (Fig. S17).

4. Conclusion

The reaction of gellan gum with thiosemicarbazide in the presence of epichlorohydrin allows synthesizing a sorbent (GEG-C) bearing carboxyl, amine and thiocarbonyl groups, which can be involved in cadmium binding; sorption properties are modulated by the pH of the

competitor ions: this is observed with both equimolar multicomponent solutions and real mining effluent (despite the huge excess of competitor metal ions). The multifunctionality of the functionalized sorbent contributes to outstanding sorption properties for cadmium removal from aqueous solutions.

This study shows the promising (fundamental) properties of this sorbent (multi-functional gellan-gum derivative) for the recovery of cadmium from diluted effluents. Obviously, the conditioning of the material (directly issued from gellan gum powder) is not appropriate for large scale application. Indeed, the micron-size of sorbent particles precludes the use of this material in fixed-bed columns (due to head loss pressure and blockage). In stirred tank reactor, the solid/liquid separation would be also hindered by the micron-sized particles. Several possibilities exist for overpassing these difficulties: (a) aggregating these particles to reach a size facilitating solid/liquid separation (with probably some limitations in mass transfer end uptake kinetics), or (b) designing gellan gum as spherical beads, which would be further functionalized [107–109].

Declaration of competing interest

The authors declare the following financial interests/personal

relationships which may be considered as potential competing interests:

Yuezhou WEI reports financial support was provided by National Natural Science Foundation of China.

Data availability

Data will be made available on request.

Acknowledgements

Y·W acknowledges the financial support of National Natural Science Foundation of China for supporting projects [U1967218, and 11975082].

Appendix A. Supplementary data

Supplementary data to this article can be found online at https://doi.org/10.1016/j.jwpe.2023.103928.

References

[1] WHO, in: W.H. Organization (Ed.), Guidelines for Drinking-water Quality, WHO, Geneva, Switzerland, 2017. http://apps.who.int/iris.
[2] M. Wang, Z. Chen, W. Song, D. Hong, L. Huang, Y. Li, A review on cadmium exposure in the population and intervention strategies against cadmium toxicity, Bull. Environ. Contam. Toxicol. 106 (2021) 65–74, https://doi.org/10.1007/s00128-020-03088-1.
[3] A. Deshwal, N. Kaur, P. Mehta, N. Thakur, A review on the effects of cadmium toxicity on living beings, J. Pharm. Res. Int. 33 (2021) 300–305, https://doi.org/10.9734/jpri/2021/v33i57A34000.
[4] M.N. Rana, J. Tangpong, M.M. Rahman, Toxicodynamics of lead, cadmium, mercury and arsenic- induced kidney toxicity and treatment strategy: a mini review, Toxicol. Rep. 5 (2018) 704–713, https://doi.org/10.1016/j.toxrep.2018.05.012.
[5] RSC, Periodic table. https://www.rsc.org/periodic-table/ (Accessed: 5/10/2021).
[6] OSHA, Safety and health topics/cadmium. https://www.osha.gov/cadmium. Accessed: 05/13/2023.
[7] S. Kouzbour, B. Gourich, F. Gros, C. Vial, F. Allam, Y. Stiriba, Comparative analysis of industrial processes for cadmium removal from phosphoric acid: a review, Hydrometallurgy 188 (2019) 222–247, https://doi.org/10.1016/j.hydromet.2019.06.014.
[8] S. Islamoglu, L. Yilmaz, H.O. Ozbelge, Development of a precipitation based separation scheme for selective removal and recovery of heavy metals from cadmium rich electroplating industry effluents, Sep. Sci. Technol. 41 (2006) 3367–3385, https://doi.org/10.1080/01496390600851665.
[9] S. Jebri, M. Jaouadi, I. Khattech, Precipitation of cadmium in water by the addition of phosphate solutions prepared from digested samples of waste animal bones, Desalin. Water Treat. 217 (2021) 253–261, https://doi.org/10.5004/dwt.2021.26899.
[10] S. Kouzbour, B. Gourich, F. Gros, C. Vial, Y. Stiriba, A novel approach for removing cadmium from synthetic wet phosphoric acid using sulfide precipitation process operating in batch and continuous modes, Miner. Eng. 187 (2022), 107809, https://doi.org/10.1016/j.mineng.2022.107809.
[11] M.K. Jha, V. Kumar, J. Jeong, J.-C. Lee, Review on solvent extraction of cadmium from various solutions, Hydrometallurgy 111-112 (2012) 1–9, https://doi.org/10.1016/j.hydromet.2011.09.001.
[12] A. Łukomska, A. Wiśniewska, Z. Dąbrowski, D. Kolasa, J. Lach, K. Wróbel, U. Domańska, New method for recovery of nickel and cadmium from the "black mass" of spent Ni-Cd batteries by solvent extraction, J. Mol. Liq. 357 (2022), 119087, https://doi.org/10.1016/j.molliq.2022.119087.
[13] R. Lommelen, K. Binnemans, Hard–soft interactions in solvent extraction with basic extractants: comparing zinc and cadmium halides, ACS Omega 6 (2021) 27924–27935, https://doi.org/10.1021/acsomega.1c03790.
[14] R. Kumar, J. Chawla, Removal of cadmium ion from water/wastewater by nano-metal oxides: a review, Water Qual. Exposure Health 5 (2014) 215–226, https://doi.org/10.1007/s12403-013-0100-8.
[15] T.A. Oyehan, T. Laoui, B. Tawabini, F. Patel, F.A. Olabemiwo, M.A. Atieh, Enhancing the adsorptive capacity of carbon nanofibers by impregnation with ferric oxide for the removal of cadmium from aqueous solution, J. Water Process Eng. 42 (2021), 102130, https://doi.org/10.1016/j.jwpe.2021.102130.
[16] R. Kumar, J. Chawla, I. Kaur, Removal of cadmium ion from wastewater by carbon-based nanosorbents: a review, J. Water Health 13 (2014) 18–33, https://doi.org/10.2166/wh.2014.024.
[17] I.A.W. Tan, J.C. Chan, B.H. Hameed, L.L.P. Lim, Adsorption behavior of cadmium ions onto phosphoric acid-impregnated microwave-induced mesoporous activated carbon, J. Water Process Eng. 14 (2016) 60–70, https://doi.org/10.1016/j.jwpe.2016.10.007.
[18] M.M. Kwikima, S. Mateso, Y. Chebude, Potentials of agricultural wastes as the ultimate alternative adsorbent for cadmium removal from wastewater. A review, Sci. Afr. 13 (2021), e00934, https://doi.org/10.1016/j.sciaf.2021.e00934.
[19] A. Akinterinwa, U. Reuben, J.U. Atiku, M. Adamu, Focus on the removal of lead and cadmium ions from aqueous solutions using starch derivatives: a review, Carbohydr. Polym. 290 (2022), 119463, https://doi.org/10.1016/j.carbpol.2022.119463.
[20] V. Kumar, S.K. Dwivedi, S. Oh, A review on microbial-integrated techniques as promising cleaner option for removal of chromium, cadmium and lead from industrial wastewater, J. Water Process Eng. 47 (2022), 102727, https://doi.org/10.1016/j.jwpe.2022.102727.
[21] E. Nishikawa, S.L. Cardoso, C.S.D. Costa, M.G.C. da Silva, M.G.A. Vieira, New perception of the continuous biosorption of cadmium on a seaweed derivative waste, J. Water Process Eng. 36 (2020), 101322, https://doi.org/10.1016/j.jwpe.2020.101322.
[22] Y. Na, J. Lee, S.H. Lee, P. Kumar, J.H. Kim, R. Patel, Removal of heavy metals by polysaccharide: a review, Polym.-Plast. Technol. Mater. 59 (2020) 1770–1790, https://doi.org/10.1080/25740881.2020.1768545.
[23] A. Bożęcka, M. Orlof-Naturalna, S. Sanak-Rydlewska, Removal of lead, cadmium and copper ions from aqueous solutions by using ion exchange resin C 160, Gospodarka Surowcami Mineralnymi, Miner. Resour. Manag. 32 (2016) 129–140, https://doi.org/10.1515/gospo-2016-0033.
[24] O.E. Roshdy, Removal of uranium, cadmium and iron ions from phosphoric acid solution using amberjet 1200 H resin: an experimental, isotherm and kinetic study, J. Radioanal. Nucl. Chem. 329 (2021) 85–101, https://doi.org/10.1007/s10967-021-07792-y.
[25] A. Tunceli, A. Ulas, O. Acar, A.R. Türker, Adsorption isotherms, kinetic and thermodynamic studies on cadmium and lead ions from water solutions using Amberlyst 15 resin, Turk. J. Chem. 46 (2022) 13, https://doi.org/10.3906/kim-2107-28.
[26] M. Marszałek, E. Knapik, M. Piotrowski, K. Chruszcz-Lipska, Removal of cadmium from phosphoric acid in the presence of chloride ions using commercially available anion exchange resins, J. Ind. Eng. Chem. 118 (2023) 488–498, https://doi.org/10.1016/j.jiec.2022.11.032.
[27] S. Elfeghe, S. Anwar, Y. Zhang, Adsorption and removal studies of cadmium ion onto sulphonic/phosphonic acid functionalization resins, Can. J. Chem. Eng. 100 (2022) 3006–3014, https://doi.org/10.1002/cjce.24400.
[28] A.A. Atia, A.M. Donia, A.M. Yousif, Synthesis of amine and thio chelating resins and study of their interaction with zinc(II), cadmium(II) and mercury(II) ions in their aqueous solutions, React. Funct. Polym. 56 (2003) 75–82, https://doi.org/10.1016/S1381-5148(03)00046-4.
[29] S. Zhu, C. Xi, Y. Zhang, F. Zhang, Preparation and characterization of cadmium (II)-ion-imprinted composites based on epoxy resin, ACS Appl. Polym. Mater. 4 (2022) 9284–9293, https://doi.org/10.1021/acsapm.2c01547.
[30] Z. Xiaowei, S. Naizhong, J. Qiong, Z. Weihong, Studies on the sorption of cadmium(II), zinc(II), and copper(II) with PTFE selective resin containing primary amine N1923 and Cyanex923, Ind. Eng. Chem. Res. 50 (2011) 4625–4630, https://doi.org/10.1021/ie101493r.
[31] N. Van Nguyen, J.-C. Lee, H.T. Huynh, J. Jeong, Extraction and separation of cadmium from the chloride solution of E-waste using Cyanex 923 impregnated Amberlite XAD-7HP resin, Mater. Trans. 56 (2015) 1294–1301, https://doi.org/10.2320/matertrans.M2015137.
[32] T. Dong, H. Xing, H. Wu, Y. Lv, L. Wu, S. Mi, L. Yang, Preparation of magnetic Levextrel resin for cadmium(II) removal, Environ. Technol. Innov. 23 (2021), 101657, https://doi.org/10.1016/j.eti.2021.101657.
[33] D.H. Fatmehsari, D. Darvishi, S. Etemadi, A.R. Eivazi Hollagh, E. Keshavarz Alamdari, A.A. Salardini, Interaction between TBP and D2EHPA during Zn, Cd, Mn, Cu, Co and Ni solvent extraction: a thermodynamic and empirical approach, Hydrometallurgy 98 (2009) 143–147, https://doi.org/10.1016/j.hydromet.2009.04.010.
[34] E. Sonmez, F. Sonmez, R.A. Kumbasar, V. Eyupoglu, Synergistic and selective extraction of Cd^{2+} from acidic solution containing Cd^{2+}, Co^{2+}, Ni^{2+} by triisooctylamine (TIOA) and tributyl phosphate (TBP), J. Ind. Eng. Chem. 18 (2012) 1286–1292, https://doi.org/10.1016/j.jiec.2012.01.025.
[35] M.B. Singh, A.J. Mukhtyar, Y.Z. Bootwala, V.G. Gaikar, Extraction of cadmium by TODGA–dodecane and TBP–dodecane: a comparative study by MD simulation, Sep. Sci. Technol. 52 (2017) 1172–1185, https://doi.org/10.1080/01496395.2017.1282967.
[36] E. Guibal, Interactions of metal ions with chitosan-based sorbents: a review, Sep. Purif. Technol. 38 (2004) 43–74, https://doi.org/10.1016/j.seppur.2003.10.004.
[37] X. Gao, C. Guo, J. Hao, Z. Zhao, H. Long, M. Li, Adsorption of heavy metal ions by sodium alginate based adsorbent-a review and new perspectives, Int. J. Biol. Macromol. 164 (2020) 4423–4434, https://doi.org/10.1016/j.ijbiomac.2020.09.046.
[38] Z.A. Sutirman, M.M. Sanagi, W.I. Wan Aini, Alginate-based adsorbents for removal of metal ions and radionuclides from aqueous solutions: a review, Int. J. Biol. Macromol. 174 (2021) 216–228, https://doi.org/10.1016/j.ijbiomac.2021.01.150.
[39] R. Kumar, R.K. Sharma, A.P. Singh, Cellulose based grafted biosorbents - journey from lignocellulose biomass to toxic metal ions sorption applications - a review, J. Mol. Liq. 232 (2017) 62–93, https://doi.org/10.1016/j.molliq.2017.02.050.
[40] Z.N. Garba, I. Lawan, W. Zhou, M. Zhang, L. Wang, Z. Yuan, Microcrystalline cellulose (MCC) based materials as emerging adsorbents for the removal of dyes and heavy metals – a review, Sci. Total Environ. 717 (2020), 135070, https://doi.org/10.1016/j.scitotenv.2019.135070.
[41] A. Kaur, D. Singh, D. Sud, A review on grafted, crosslinked and composites of biopolymer Xanthan gum for phasing out synthetic dyes and toxic metal ions from aqueous solutions, J. Polym. Res. 27 (2020) 297, https://doi.org/10.1007/s10965-020-02271-6.

[42] K.M. Zia, S. Tabasum, M.F. Khan, N. Akram, N. Akhter, A. Noreen, M. Zuber, Recent trends on gellan gum blends with natural and synthetic polymers: a review, Int. J. Biol. Macromol. 109 (2018) 1068–1087, https://doi.org/10.1016/j.ijbiomac.2017.11.099.
[43] K. Balíková, B. Farkas, P. Matúš, M. Urík, Prospects of biogenic xanthan and gellan in removal of heavy metals from contaminated waters, Polymers 14 (2022) 5326.
[44] N. Lázaro, A.L. Sevilla, S. Morales, A.M. Marqués, Heavy metal biosorption by gellan gum gel beads, Water Res. 37 (2003) 2118–2126, https://doi.org/10.1016/S0043-1354(02)00575-4.
[45] V.S. Pandey, S.K. Verma, M. Yadav, K. Behari, Studies on graft copolymerization of gellan gum with N,N-dimethylacrylamide by the redox system, Int. J. Biol. Macromol. 70 (2014) 108–115, https://doi.org/10.1016/j.ijbiomac.2014.06.043.
[46] S.K. Verma, V.S. Pandey, M.Y.K. Behari, Gellan gum-g-N-vinyl-2-pyrrolidone: synthesis, swelling, metal ion uptake and flocculation behavior, Int. J. Biol. Macromol. 72 (2015) 1292–1300, https://doi.org/10.1016/j.ijbiomac.2014.10.036.
[47] K.T. Giri, K.B. Yadav, H. Badwaik, Synthesis and characterization of gellan gum based bioadsorbent for wastewater treatment, Curr. Microwave Chem. 5 (2018) 84–96, https://doi.org/10.2174/2213335605666180319123536.
[48] S. Racovita, M.-A. Lungan, A.-L. Vasiliu, S. Vasiliu, M. Mihai, Sorption behavior of grafted porous microparticles based on methacrylic monomers and chitosan/gellan gum towards copper(II) and nickel(II) ions in aqueous solutions, ChemistrySelect 6 (2021) 12512–12523, https://doi.org/10.1002/slct.202103223.
[49] D. Kang, F. Zhang, H. Zhang, Fabrication of stable aqueous dispersions of graphene using gellan gum as a reducing and stabilizing agent and its nanohybrids, Mater. Chem. Phys. 149-150 (2015) 129–139, https://doi.org/10.1016/j.matchemphys.2014.09.055.
[50] C. Modrogan, A.M. Pandele, C. Bobirică, D. Dobrotă, A.M. Dăncilă, G. Gârleanu, O.D. Orbuleț, C. Borda, D. Gârleanu, C. Orbeci, Synthesis, characterization and sorption capacity examination for a novel hydrogel composite based on gellan gum and graphene oxide (GG/GO), Polymers 12 (2020) 1182, https://doi.org/10.3390/polym12051182.
[51] G. Shukla, R.C. Ferrier Jr., The versatile, functional polyether, polyepichlorohydrin: history, synthesis, and applications, J. Polym. Sci. 59 (2021) 2704–2718, https://doi.org/10.1002/pol.20210514.
[52] S.D. Alexandratos, X. Zhu, Polyols as scaffolds in the development of ion-selective polymer-supported reagents: the effect of auxiliary groups on the mechanism of metal ion complexation, Inorg. Chem. 47 (2008) 2831–2836, https://doi.org/10.1021/ic702263x.
[53] V.V. Kulkarni, A.K. Golder, P.K. Ghosh, Synergistic effect using a functionalized dual-site adsorbent in Pb(II) and Cu(II) uptake and comparison with mono-site resins, J. Water Process Eng. 18 (2017) 92–101, https://doi.org/10.1016/j.jwpe.2017.06.009.
[54] M.F. Hamza, K.A.M. Salih, K. Zhou, Y. Wei, H.A. Abu Khoziem, S.H. Alotaibi, E. Guibal, Effect of bi-functionalization of algal/polyethyleneimine composite beads on the enhancement of tungstate sorption: application to metal recovery from ore leachate, Sep. Purif. Technol. 290 (2022), 120893, https://doi.org/10.1016/j.seppur.2022.120893.
[55] X. Guo, Y. Feng, L. Ma, D. Gao, J. Jing, J. Yu, H. Sun, H. Gong, Y. Zhang, Phosphoryl functionalized mesoporous silica for uranium adsorption, Appl. Surf. Sci. 402 (2017) 53–60, https://doi.org/10.1016/j.apsusc.2017.01.050.
[56] M.V. Lopez-Ramon, F. Stoeckli, C. Moreno-Castilla, F. Carrasco-Marin, On the characterization of acidic and basic surface sites on carbons by various techniques, Carbon 37 (1999) 1215–1221, https://doi.org/10.1016/s0008-6223(98)00317-0.
[57] Y.S. Ho, G. McKay, Pseudo-second order model for sorption processes, Process Biochem. 34 (1999) 451–465, https://doi.org/10.1016/S0032-9592(98)00112-5.
[58] J. Crank, The Mathematics of Diffusion, 2nd. ed., Oxford University Press, Oxford, U.K., 1975, p. 414.
[59] C. Tien, Adsorption Calculations and Modeling, Butterworth-Heinemann, Newton, MA, 1994, p. 243.
[60] C.S.T. Araujo, I.L.S. Almeida, H.C. Rezende, S. Marcionilio, J.J.L. Leon, T.N. de Matos, Elucidation of mechanism involved in adsorption of Pb(II) onto lobeira fruit (Solanum lycocarpum) using Langmuir, Freundlich and Temkin isotherms, Microchem. J. 137 (2018) 348–354, https://doi.org/10.1016/j.microc.2017.11.009.
[61] K.H. Chu, Revisiting the Temkin isotherm: dimensional inconsistency and approximate forms, Ind. Eng. Chem. Res. 60 (2021) 13140–13147, https://doi.org/10.1021/acs.iecr.1c01788.
[62] V. Puccia, M.J. Avena, On the use of the Dubinin-Radushkevich equation to distinguish between physical and chemical adsorption at the solid-water interface, Colloid Interface Sci. Commun. 41 (2021), 100376, https://doi.org/10.1016/j.colcom.2021.100376.
[63] R.R. Escudero, M. Robitzer, F. Di Renzo, F. Quignard, Alginate aerogels as adsorbents of polar molecules from liquid hydrocarbons: Hexanol as probe molecule, Carbohydr. Polym. 75 (2009) 52–57, https://doi.org/10.1016/j.carbpol.2008.06.008.
[64] M. Thommes, K. Kaneko, A.V. Neimark, J.P. Olivier, F. Rodriguez-Reinoso, J. Rouquerol, K.S.W. Sing, Physisorption of gases, with special reference to the evaluation of surface area and pore size distribution (IUPAC technical report), Pure Appl. Chem. 87 (2015) 1051–1069, https://doi.org/10.1515/pac-2014-1117.
[65] A. Abbasi, S. Ikram, Fabrication of a novel green bio-composite for sequestration of Victoria Blue from aquatic medium: isotherm, kinetics, and thermodynamic investigations, Chem. Phys. Lett. 800 (2022), 139665, https://doi.org/10.1016/j.cplett.2022.139665.
[66] L. Liang, X. Lin, Y. Liu, S. Sun, H. Chu, Y. Chen, D. Liu, X. Luo, J. Zhang, R. Shang, Carboxymethyl konjac glucomannan mechanically reinforcing gellan gum microspheres for uranium removal, Int. J. Biol. Macromol. 145 (2020) 535–546, https://doi.org/10.1016/j.ijbiomac.2019.12.188.
[67] J. Green, A review of phosphorus-containing flame retardants, J. Fire Sci. 10 (1992) 470–487, https://doi.org/10.1177/073490419201000602.
[68] S. Aafrin Hazaana, A. Joseph, S. Selvasekarapandian, R. Meera Naachiyar, M. Vengadesh Krishna, N. Muniraj Vignesh, Development and characterization of biopolymer electrolyte based on gellan gum (GG) with lithium chloride (LiCl) for the application of electrochemical devices, Polym. Bull. 80 (2023) 5291–5311, https://doi.org/10.1007/s00289-022-04316-w.
[69] N.B. Colthup, L.H. Daly, S.E. Wiberley, Introduction to Infrared and Raman Spectroscopy, 3rd. ed., Academic Press, Inc, San Diego, CA (USA), 1990, p. 560.
[70] B. Thilaga Rajeswari, P. Sathya, P. Dhanasekaran, G. Vinitha, S. Meyvel, V. Vijayalakshmi, J. Aarthi, First-time investigation on crystal growth, optical, thermal, electrical and third-order non-linear optical activities of novel thiosemicarbazide single crystals for non-linear optical applications, J. Mater. Sci. Mater. Electron. 32 (2021) 22984–22998, https://doi.org/10.1007/s10854-021-06783-9.
[71] A.M. Azzam, M.A. Shenashen, M.M. Selim, H. Yamaguchi, I.M. El-Sewify, S. Kawada, A.A. Alhamid, S.A. El-Safty, Nanospherical inorganic α-Fe core-organic shell necklaces for the removal of arsenic(V) and chromium(VI) from aqueous solution, J. Phys. Chem. Solids 109 (2017) 78–88, https://doi.org/10.1016/j.jpcs.2017.05.017.
[72] H.T. Nguyen, F.A. Ngwabebhoh, N. Saha, T. Saha, P. Saha, Gellan gum/bacterial cellulose hydrogel crosslinked with citric acid as an eco-friendly green adsorbent for safranin and crystal violet dye removal, Int. J. Biol. Macromol. 222 (2022) 77–89, https://doi.org/10.1016/j.ijbiomac.2022.09.040.
[73] L.H. Fasolin, C.S.F. Picone, R.C. Santana, R.L. Cunha, Production of hybrid gels from polysorbate and gellan gum, Food Res. Int. 54 (2013) 501–507, https://doi.org/10.1016/j.foodres.2013.07.026.
[74] M. Cassanelli, V. Prosapio, I. Norton, T. Mills, Acidified/basified gellan gum gels: the role of the structure in drying/rehydration mechanisms, Food Hydrocoll. 82 (2018) 346–354, https://doi.org/10.1016/j.foodhyd.2018.04.024.
[75] R. Williams, pKa data (compiled by R. Williams). http://www.chem.wisc.edu/areas/reich/pkatable/pKa_compilation-1-Williams.pdf. Accessed: 4/6/2017.
[76] A. Mellah, D. Benachour, The solvent extraction of zinc, cadmium and chromium from phosphoric acid solutions by tri-n butyl phosphate in kerosene diluent, Sep. Purif. Technol. 56 (2007) 220–224, https://doi.org/10.1016/j.seppur.2007.01.037.
[77] M.M. Montazer-Rahmati, P. Rabbani, A. Abdolali, A.R. Keshtkar, Kinetics and equilibrium studies on biosorption of cadmium, lead, and nickel ions from aqueous solutions by intact and chemically modified brown algae, J. Hazard. Mater. 185 (2011) 401–407, https://doi.org/10.1016/j.jhazmat.2010.09.047.
[78] M. Aliabadi, M. Irani, J. Ismaeili, H. Piri, M.J. Parnian, Electrospun nanofiber membrane of PEO/chitosan for the adsorption of nickel, cadmium, lead and copper ions from aqueous solution, Chem. Eng. J. 220 (2013) 237–243, https://doi.org/10.1016/j.cej.2013.01.021.
[79] A. Jakóbik-Kolon, J. Bok-Badura, A.K. Milewski, K. Mitko, Sorption studies of cadmium and lead ions on hybrid polysaccharide biosorbents, Sep. Sci. Technol. 53 (2018) 1132–1141, https://doi.org/10.1080/01496395.2017.1298613.
[80] T.R. Maki, B.H. Qasim, Potassium hydroxide activated peanut shell as an effective adsorbent for the removal of zinc, lead and cadmium from wastewater, J. Ecol. Eng. 24 (2023) 66–78, https://doi.org/10.12911/22998993/156006.
[81] M.F. Hamza, Y. Wei, A. Benettayeb, X. Wang, E. Guibal, Efficient removal of uranium, cadmium and mercury from aqueous solutions using grafted hydrazide-micro-magnetite chitosan derivative, J. Mater. Sci. 55 (2020) 4193–4212, https://doi.org/10.1007/s10853-019-04235-8.
[82] Y. Marcus, Ion Properties, Marcel Dekker, Inc, New York, NY, 1997, p. 259.
[83] E. Nieboer, D.H.S. Richardson, The replacement of the non-descript therm heavy-metals by a biologically and chemically significant classification of metal-ions, Environ. Pollut. Ser. B 1 (1980) 3–26, https://doi.org/10.1016/0143-148x(80)90017-8.
[84] R.G. Pearson, Acids and bases, Science (New York, N.Y.) 151 (1966) 172–177, https://doi.org/10.1126/science.151.3707.172.
[85] Q. Hu, Z. Zhang, Application of Dubinin–Radushkevich isotherm model at the solid/solution interface: a theoretical analysis, J. Mol. Liq. 277 (2019) 646–648, https://doi.org/10.1016/j.molliq.2019.01.005.
[86] S. Mushtaq, F.E. Bareen, A. Tayyeb, Equilibrium kinetics and thermodynamic studies on biosorption of heavy metals by metal-resistant strains of Trichoderma isolated from tannery solid waste, Environ. Sci. Pollut. Res. 30 (2023) 10925–10954, https://doi.org/10.1007/s11356-022-22860-w.
[87] D. Bilba, N. Bilba, M. Albu, Kinetics of cadmium ion sorption on ion exchange and chelating resins, Solvent Extr. Ion Exch. 17 (1999) 1557–1569, https://doi.org/10.1080/07366299908934665.
[88] M. Khalil, Y.F. El-Aryan, E.A. Abdel-Galil, Equilibrium studies on the removal of cadmium ion on amberlite IR-120 sorbent, Colloid J. 77 (2015) 745–753, https://doi.org/10.1134/s1061933x15060113.
[89] S. Wu, K. Zhang, X. Wang, Y. Jia, B. Sun, T. Luo, F. Meng, Z. Jin, D. Lin, W. Shen, et al., Enhanced adsorption of cadmium ions by 3D sulfonated reduced graphene oxide, Chem. Eng. J. 262 (2015) 1292–1302, https://doi.org/10.1016/j.cej.2014.10.092.
[90] Y. Zhou, N. Xu, K. Tian, T. Qing, Y. Hao, P. Liang, M. Li, Nitrilotriacetic acid modified magnetic Prussian blue for efficient removal of cadmium from

wastewater, Appl. Surf. Sci. 600 (2022), 154102, https://doi.org/10.1016/j.apsusc.2022.154102.
[91] L.P. Lingamdinne, V.R. Lebaka, J.R. Koduru, Y.-Y. Chang, Insights into manganese ferrite anchored graphene oxide to remove Cd(II) and U(VI) via batch and semi-batch columns and its potential antibacterial applications, Chemosphere 310 (2023), 136888, https://doi.org/10.1016/j.chemosphere.2022.136888.
[92] S.M.A. Abasiyan, F. Dashbolaghi, G.R. Mahdavinia, Chitosan cross-linked with κ-carrageenan to remove cadmium from water and soil systems, Environ. Sci. Pollut. Res. 26 (2019) 26254–26264, https://doi.org/10.1007/s11356-019-05488-1.
[93] M.H. Taha, A.M. Masoud, Y.M. Khawassek, A.E.M. Hussein, H.F. Aly, E. Guibal, Cadmium and iron removal from phosphoric acid using commercial resins for purification purpose, Environ. Sci. Pollut. Res. 27 (2020) 31278–31288, https://doi.org/10.1007/s11356-020-09342-7.
[94] A. Jakóbik-Kolon, A.K. Milewski, K. Mitko, A. Lis, Preparation of pectin-based biosorbents for cadmium and lead ions removal, Sep. Sci. Technol. 49 (2014) 1679–1688, https://doi.org/10.1080/01496395.2014.906469.
[95] A. Jakóbik-Kolon, J. Bok-Badura, Sorption and desorption of cadmium and lead on pectin-based biosorbents – batch and column studies, Sep. Sci. Technol. 55 (2020) 2108–2121, https://doi.org/10.1080/01496395.2019.1583253.
[96] D. Bulgariu, L. Bulgariu, Potential use of alkaline treated algae waste biomass as sustainable biosorbent for clean recovery of cadmium(II) from aqueous media: batch and column studies, J. Clean. Prod. 112 (2016) 4525–4533, https://doi.org/10.1016/j.jclepro.2015.05.124.
[97] Y. Wang, R. Zhou, C. Wang, G. Zhou, C. Hua, Y. Cao, Z. Song, Novel environmental-friendly nano-composite magnetic attapulgite functionalized by chitosan and EDTA for cadmium (II) removal, J. Alloys Compd. 817 (2020), 153286, https://doi.org/10.1016/j.jallcom.2019.153286.
[98] C.P. Tatara, M.C. Newman, J.T. McCloskey, P.L. Williams, Use of ion characteristics to predict relative toxicity of mono-, di- and trivalent metal ions: Caenorhabditis elegans LC50, Aquat. Toxicol. 42 (1998) 255–269, https://doi.org/10.1016/S0166-445X(97)00104-5.
[99] M. Spinti, H. Zhuang, E.M. Trujillo, Evaluation of immobilized biomass beads for removing heavy metals from wastewaters, Water Environ. Res. 67 (1995) 943–952, https://doi.org/10.2175/106143095X133176.
[100] V. Beaugeard, J. Muller, A. Graillot, X. Ding, J.-J. Robin, S. Monge, Acidic polymeric sorbents for the removal of metallic pollution in water: a review, React. Funct. Polym. 152 (2020), 104599, https://doi.org/10.1016/j.reactfunctpolym.2020.104599.
[101] M. Misono, E.I. Ochiai, Y. Saito, Y. Yoneda, A new dual parameter scale for the strength of Lewis acids and bases with the evaluation of their softness, J. Inorg. Nucl. Chem. 29 (1967) 2685–2691, https://doi.org/10.1016/0022-1902(67)80006-X.
[102] N.H. Elsayed, M. Monier, R.A.S. Alatawi, Thiosemicarbazide-modified/ion-imprinted phenolic resin for selective uptake of cadmium ions, Mater. Chem. Phys. 264 (2021), 124433, https://doi.org/10.1016/j.matchemphys.2021.124433.
[103] A. Murat, L. Wang, S. Abliz, A. Yimit, Preparation, characterization of cd(II) ion-imprinted microsphere and its selectivity for template ion, Coatings 12 (2022) 1038, https://doi.org/10.3390/coatings12081038.
[104] X. Hu, L. Yan, Y. Wang, M. Xu, Ice segregation induced self-assembly of salecan and grapheme oxide nanosheets into ion-imprinted aerogel with superior selectivity for cadmium (II) capture, Chem. Eng. J. 417 (2021), 128106, https://doi.org/10.1016/j.cej.2020.128106.
[105] P.R. Varadwaj, A. Varadwaj, B.-Y. Jin, Ligand(s)-to-metal charge transfer as a factor controlling the equilibrium constants of late first-row transition metal complexes: revealing the Irving–Williams thermodynamical series, Phys. Chem. Chem. Phys. 17 (2015) 805–811, https://doi.org/10.1039/C4CP03953J.
[106] H. Jeong, H. Kim, T. Jang, Irrigation water quality standards for indirect wastewater reuse in agriculture: a contribution toward sustainable wastewater reuse in South Korea, Water 8 (2016), art.169, https://doi.org/10.3390/w8040169.
[107] D. Gomes, D. Costa, J.A. Queiroz, L.A. Passarinha, A. Sousa, A new insight in gellan microspheres application to capture a plasmid DNA vaccine from an *Escherichia coli* lysate, Sep. Purif. Technol. 274 (2021), 119013, https://doi.org/10.1016/j.seppur.2021.119013.
[108] J.A. Pires Vilela, F.P. Bonsanto, R.L. Cunha, Mechanical properties of gellan gum beads prepared with potassium or calcium ions, J. Texture Stud. 53 (2022) 531–539, https://doi.org/10.1111/jtxs.12684.
[109] X. Wang, C. Zohar-Perez, Y. Zeng, Y. Zou, Y. Chen, S. Wu, Y. Wang, S. Arazi, A. Nussinovitch, Y. Achmon, Assessment of the environmental impact of agar, alginate, and gellan gum carbohydrate gum macro beads biodegradation in a simulated agricultural field system, Environ. Technol. Innov. 30 (2023), 103034, https://doi.org/10.1016/j.eti.2023.103034.